KIF13A mediates the activity-dependent transport of ESCRT-0 proteins in axons

Veronica Birdsall[1], Yuuta Imoto[2], Shigeki Watanabe[2,3], Clarissa L. Waites[4,5]

1. Neurobiology and Behavior PhD program, Columbia University, New York, NY 10027

2. Department of Cell Biology, Johns Hopkins University, Baltimore, MD 21205

3. Solomon H. Snyder Department of Neuroscience, Johns Hopkins University, MD 21205, USA

4. Department of Pathology and Cell Biology, Columbia University Medical Center, New York, NY 10032

5. Department of Neuroscience, Columbia University, New York, NY 10027

Correspondence to:

Clarissa Waites, Ph.D., Departments of Pathology & Cell Biology and Neuroscience,

650 W. 168th St., Black Building 1210B, New York, NY 10032, USA; Tel. 212-305-6025;

e-mail: cw2622@cumc.columbia.edu

Running title: Activity-dependent transport of ESCRT-0 proteins

Abstract

Turnover of synaptic vesicle (SV) proteins is vital for the maintenance of healthy, functional synapses in neurons. Our previous work showed that the degradation of SV proteins is mediated by the endosomal sorting complex required for transport (ESCRT) pathway in an activity-dependent manner. Here, we characterize the axonal transport dynamics of ESCRT-0 proteins Hrs and STAM1, the first components of the ESCRT pathway critical for initiating SV protein degradation. Hrs- and STAM1-positive transport vesicles exhibit increased anterograde and bidirectional motility in response to neuronal firing, and frequent colocalization with SV pools. These ESCRT-0 vesicles are a subset of Rab5-positive structures in axons, likely representing pro-degradative early endosomes. Further, we identify kinesin motor protein KIF13A as essential for the activity-dependent transport of ESCRT-0 vesicles as well as the degradation of SV membrane proteins. Together, these data demonstrate a novel KIF13A-dependent mechanism for mobilizing axonal transport of ESCRT machinery to facilitate the degradation of SV proteins.

Introduction

Synaptic vesicles (SVs) are the fundamental units of neurotransmitter storage and release, and as such their efficient fusion and recycling are essential for neuronal communication. These processes depend upon maintaining the proper complement of functional SV membrane proteins, as the inability to clear damaged or misfolded SV proteins can precipitate synaptic dysfunction and neurodegeneration (Bezprozvanny and Hiesinger 2013; Esposito, Ana Clara, and Verstreken 2012; Hall et al. 2017). However, the elaborate morphology of neurons creates unique spatial challenges for SV protein clearance and degradation. First, lysosomes - the degradative organelles for SV membrane proteins - are primarily localized to neuronal cell bodies, requiring retrograde transport of SV proteins destined for degradation. Second, the machinery responsible for packaging and delivering SV proteins to lysosomes must be anterogradely transported to presynaptic boutons, which often exist meters away from the cell body. In addition to these spatial challenges, neurons face temporal challenges in transporting degradative machinery in response to stimuli such as synaptic activity. For instance, degradative organelles (proteasomes, lysosomes, and autophagosomes) undergo activity-dependent recruitment into the postsynaptic compartment as part of the mechanism for synaptic plasticity (Bingol and Schuman 2006; Goo et al. 2017; Shehata et al. 2012), and must be rapidly mobilized to these sites. Similarly, the turnover of SV and other presynaptic proteins is stimulated by neuronal activity (Sheehan et al. 2016; Truckenbrodt et al. 2018), requiring the local presence of degradative machinery to facilitate clearance of old and damaged proteins. However, very little is known about whether or how neurons regulate the transport and delivery of this machinery to presynaptic terminals.

Previous work from our group and others has demonstrated that the degradation of SV membrane proteins requires the endosomal sorting complex required for transport (ESCRT) pathway (Sheehan et al. 2016; Uytterhoeven et al. 2011). Comprising a series of protein complexes (ESCRT-0, -I, -II, -III, Vps4), the ESCRT pathway recruits ubiquitinated membrane proteins and forms multivesicular bodies (MVBs) for delivery of this cargo to lysosomes (Hurley 2015). In addition to its degradative function, the ESCRT pathway also functions in other cellular processes, including cytokinesis and plasma membrane repair (Stoten and Carlton 2018; McCullough, Frost, and Sundquist 2018; Christ et al. 2017; Jimenez et al. 2014). Mutation or dysfunction of ESCRT-associated proteins leads to neurodegeneration in animal models (Tamai et al. 2008; J. A. Lee et al. 2007; D. Lee et al. 2019) and is linked to frontotemporal dementia (FTD)(Skibinski et al. 2005; J. A. Lee et al. 2007), amyotrophic lateral sclerosis (ALS)(Parkinson et al. 2006) and infantile-lethal epilepsy (Hall et al. 2017). Moreover, the ESCRT pathway is

essential for endosomal protein trafficking, and is implicated in the etiology of Alzheimer's and Parkinson's diseases (Vaz-Silva et al. 2018; Borland and Vilhardt 2017; Vagnozzi and Praticò 2019; Feng et al. 2020; Spencer et al. 2014, 2016). Yet despite the essential role of the ESCRT pathway in protein degradation and other cellular processes, as well as its links to neurodegenerative disease, little is known about its substrates, dynamic behavior, or mechanisms of localization and regulation in neurons.

Our previous study demonstrated that a subset of SV proteins are degraded in an activity-dependent manner, and that this process is initiated by the activation of small GTPase Rab35 and the recruitment of its effector, ESCRT-0 component Hrs (Sheehan et al. 2016). As the first component of the ESCRT pathway, Hrs functions to sequester ubiquitinated proteins destined for degradation, and to recruit downstream ESCRT machinery to promote MVB biogenesis. Interestingly, neuronal activity significantly increases the localization of Hrs to axons and SV pools, suggesting that ESCRT-0 proteins could be transported to SV pools in an activity-dependent manner to catalyze SV protein degradation. However, it is not clear how ESCRT-0 proteins are transported into and out of synapses.

In the current study, we use live imaging to further characterize ESCRT-0 protein localization and transport in axons. We find that ESCRT-0 proteins Hrs and STAM1 are transported on vesicles that exhibit activity-induced anterograde and bidirectional motility, and frequent contact with SV pools. These ESCRT-0 vesicles are Rab5-positive and likely comprise a subset of 'pro-degradative' endosomes. In addition, we identify kinesin motor protein KIF13A as essential for ESCRT-mediated degradation, since KIF13A knockdown inhibits both the activity-induced transport of Hrs and STAM1 as well as the degradation of SV proteins. Together, these findings illuminate critical spatiotemporal mechanisms of ESCRT-0 protein transport and delivery to presynaptic boutons in order to facilitate SV protein degradation.

Results

Neuronal activity increases the density of presynaptic endosomes

In our previous study, we demonstrated that neuronal firing increases the recruitment of ESCRT proteins into axons and their colocalization with SV markers (Sheehan et al. 2016). Given the role of ESCRT proteins in catalyzing MVB formation (Raiborg, Rusten, and Stenmark 2003), these changes in ESCRT protein localization may increase the numbers of MVBs and other endosomal structures at presynaptic boutons. We therefore examined electron micrographs of boutons from 16-21 day *in vitro* (DIV) hippocampal neurons treated with tetrodotoxin (TTX) to reduce neuronal firing or gabazine to increase firing. We observed a significantly higher density

of presynaptic MVBs and endosomes (defined as single-membrane structures >80 nm in diameter) following gabazine versus TTX treatment (Fig. 1A, C), suggesting that neuronal activity promotes the appearance of these structures at presynaptic boutons. Since other studies have reported that neuronal firing stimulates the biogenesis of autophagosomes at presynaptic terminals (Wang et al. 2015), we also counted the number of multilamellar structures present under each condition. Interestingly, not only was the average density of these structures lower than that of endosomes/MVBs regardless of activity level (~0.1 multilamellar structures/μm^2 vs. ~1 endosomes/μm^2 at baseline), but there was no increase in their density with gabazine treatment (Fig. 1B, D), indicating that prolonged neuronal activity specifically increases the number of endosomal structures and MVBs at presynaptic boutons (Sheehan et al. 2016).

Neuronal activity stimulates the anterograde and bidirectional transport of Hrs

These EM findings, together with our previous work (Sheehan et al. 2016), led us to hypothesize that ESCRT proteins undergo activity-dependent changes in their motility and transport to synapses. ESCRT-0 protein Hrs is the first component of the ESCRT pathway, responsible for sequestering ubiquitinated cargo and recruiting subsequent ESCRT machinery, steps that necessarily precede endolysosomal degradation of SV and other membrane proteins. Thus, we first examined the axonal transport dynamics of Hrs. To facilitate analysis of the directional movement of Hrs and other proteins, we utilized tripartite microfluidic chambers that isolate neuronal cell bodies from axons while enabling synapse formation between neurons in adjacent compartments (Fig. S1A). Lentiviral transduction of cell bodies in these chambers led to moderate protein expression levels and consistent transduction efficiency across constructs used in this study (~50%; Fig. S1B). Hippocampal neurons were transduced on 7 DIV with RFP-Hrs, and live imaging performed on 13-15 DIV. Imaging was performed either immediately following application of DMSO (control) or bicuculline and 4-aminopyridine (acute bic/4AP), or after 2 hours of treatment with these drugs (2h bic/4AP)(Fig. 2A-C; Videos 1&2). Bic/4AP treatments did not cause any detectable changes in neuronal health or increase cell death over this timeframe (Fig. S1C). Under control conditions, we observed that >60% of Hrs puncta were stationary over the course of the ~4-minute imaging session (Fig. 2A, D, F). Acute treatment with bic/4AP led to a slight but significant increase in puncta motility (from ~38% to ~50% motile), with the effect growing stronger after 2h of treatment (~60% motile puncta; Fig. 2A-D, F). No change in speed was observed across the three conditions (Fig. 2E), indicating that activity leads to the recruitment of Hrs puncta into the motile pool rather than to a fundamental change

in the mechanism of transport. Interestingly, dampening neuronal activity with 2h TTX treatment did not conversely decrease Hrs motility (Fig. S1D), indicating that basal activity levels in these cultures are low.

Like other early endosome-associated proteins (*e.g.* Rab5)(Goto-Silva et al. 2019), Hrs exhibits a mixture of anterograde, retrograde, and non-processive bidirectional motility (Fig. 2F). However, we found that only anterograde and bidirectional motility increased following treatment with bic/4AP (Fig. 2F), suggesting that neuronal activity preferentially mobilizes Hrs towards distal axonal and presynaptic sites. To investigate whether this mobilization led to increased Hrs contact with SV pools, we co-transfected dissociated hippocampal neurons with RFP-Hrs and EGFP-Synapsin (to label SV pools/presynaptic boutons (Leal-Ortiz et al. 2008)), and performed live imaging to assess colocalization between motile Hrs and stationary Synapsin puncta in axons. While we did observe motile Hrs puncta colocalizing with Synapsin at presynaptic sites (Fig. 2G-H, Video 3), this behavior did not depend upon neuronal activity, as motile Hrs puncta spent ~35% of their time in contact with Synapsin regardless of activity condition (Fig. 2G). However, Hrs/Synapsin colocalization was significantly increased following 2h of treatment with PR619, a deubiquitinating enzyme inhibitor that promotes SV protein ubiquitination (Fig. S1E-F), suggesting that Hrs interaction with presynaptic sites is ubiquitin-dependent. This finding is consistent with the role of Hrs in binding ubiquitinated proteins and sorting them toward MVBs.

To examine the morphology of Hrs-positive vesicles in axons, we performed correlative-light electron microscopy on cultured neurons lentivirally co-transduced with vesicular glutamate transporter (vGlut1-GFP) to label SV pools and HaloTag-Hrs. Intriguingly, Hrs-positive structures identified in the axon appear to be degradative in nature, including an endosome and a multivesicular body (Fig. S2). These data, along with our previous findings (Sheehan et al. 2016), suggest that Hrs undergoes activity-dependent transport in axons and is associated with degradative structures.

Neuronal activity differentially affects the motility of STAM1+ and Rab5+ vesicles

Hrs typically associates with early endosomes (Sun et al. 2003; Raiborg, Rusten, and Stenmark 2003; Flores-Rodriguez et al. 2015; Raiborg et al. 2001); thus, we next examined whether other early endosomal proteins exhibited similar transport dynamics and activity-dependent motility. One such protein is STAM1, which is recruited to endosomal membranes by Hrs to form the heterotetrameric ESCRT-0 complex (Mayers et al. 2011; Takahashi et al. 2015). We found that STAM1, like Hrs, has a punctate pattern of expression in axons, with similar dynamics to Hrs at baseline (~40% of puncta motile; Fig. 3A-C, Videos 4&5) and an even larger increase in motility

after 2h of bic/4AP (~80% motile; Fig. 3D). Also similar to Hrs, bic/4AP treatment did not alter the average speed of motile STAM1 puncta, which remained ~0.3 μm/second (Fig. 3E). The increase in fraction of anterogradely moving puncta was even more pronounced for STAM1 than for Hrs, and was accompanied by an increase in retrograde puncta movement (Fig. 3K). These findings indicate that the motility of the entire ESCRT-0 complex is sensitive to neuronal firing.

Along with the ESCRT-0 complex, another key component of early endosomes, critical for their formation and function, is the small GTPase Rab5 (Gorvel et al. 1991; Deinhardt et al. 2006; Poteryaev et al. 2010). We therefore investigated the motility of Rab5 under control and activity conditions. We found that Rab5 exhibited higher motility under control conditions than ESCRT-0 proteins (~60% motile puncta at baseline; Fig. 3I, Video 6), and that the motility of Rab5 puncta did not increase with acute bic/4AP treatment (Fig. 3F-G, I), in contrast to Hrs and STAM1. However, after 2h of bic/4AP, Rab5 puncta exhibited significantly increased motility, to ~80% motile puncta (Fig. 3F-H, I, Video 7). As with Hrs and STAM1, the average speed of Rab5 puncta was unaffected by activity treatment (Fig. 3J). The proportion of anterogradely moving Rab5 puncta also increased significantly after 2h of bic/4AP treatment (Fig. 3L), and was the only observed change in Rab5 directional movement. These data show that while Rab5 puncta do exhibit activity-dependent changes in axonal motility, this effect is more robust for ESCRT-0 proteins.

Hrs is present on a subset of axonal Rab5+ vesicles

Since the axonal dynamics of Rab5 do not precisely align with those of ESCRT-0 proteins, we next investigated whether Hrs is present on the same vesicles as Rab5 in axons. Here, we performed time-lapse imaging of axons from dissociated neurons co-transfected with RFP-Hrs and EGFP-Rab5 (Fig. 4A). The density of Rab5 puncta in co-transfected axons was on average higher than that of Hrs puncta, and while >80% of Hrs puncta (stationary and motile) were also positive for Rab5 (Fig. 4B,E), the converse was not true. Indeed, only ~40% of stationary Rab5 puncta and ~60% of motile Rab5 puncta were positive for Hrs (Fig. 4C, F). These data suggest that Hrs is present on a subset of Rab5+ structures, consistent with previous studies showing that Rab5 is associated with a heterogenous population of endosomes as well as SVs (Simonsen et al. 1998; Christoforidis et al. 1999; Flores-Rodriguez et al. 2015; Fischer von Mollard et al. 1994; Shimizu, Kawamura, and Ozaki 2003; Zhang et al. 2013). Moreover, while the total number (stationary and motile) of Hrs+/Rab5+ puncta did not change in response to neuronal activity (Fig. 4D), the number of motile Hrs+/Rab5+ puncta increased significantly (Fig.

4G). These findings indicate that an Hrs+ subset of Rab5 vesicles is responsive to neuronal firing, providing a potential explanation for why the total population of axonal Rab5 shows only a modest increase in motility in response to bic/4AP treatment (Fig. 3I).

Given our previous findings that Rab35 is present on the same vesicles as Hrs and required for activity-dependent degradation of SV proteins (Sheehan et al. 2016), we also investigated the axonal transport dynamics of Rab35. We found that Rab35 exhibited higher motility than Hrs at baseline (~60% motile, Fig. S3D,F), but no change in motility in response to bic/4AP, even after 2h of treatment (Fig. S3D,F). However, the colocalization between RFP-Hrs and EGFP-Rab35 in axons increased slightly but significantly in response to 2h bic/4AP (Fig. S3G-H). These data, along with similarities in the directional transport profiles of Hrs and Rab35 following 2h bic/4AP treatment (Fig. 2F and Fig. S3F), suggest that Rab35 may colocalize more strongly with the motile pool of Hrs, but that Rab35 motility is not regulated by neuronal firing in the same way.

Hrs association with vesicles requires the FYVE domain and occurs in the somatodendritic compartment

Studies in non-neuronal cells show that Hrs recruitment to endosomal membranes depends on interactions between its FYVE domain and the endosome-enriched lipid phosphoinositol-3-phosphate (PI3P)(Komada & Soriano 1999; Stahelin et al. 2002). However, other domains of Hrs, in particular the C-terminal coiled-coil domain, have also been reported to facilitate its membrane targeting (Hayakawa & Kitamura 2000; Raiborg et al. 2001). Given the dearth of evidence about axonal targeting of Hrs, and reports that EEA1, another FYVE domain-containing early endosomal protein, is not present in axons (Gaullier et al. 2000; Lawe et al. 2000; Wilson et al. 2000), we wanted to investigate whether the FYVE/PI3P interaction was required for targeting Hrs to motile vesicles in axons. We first assessed whether the axonal dynamics of the Hrs FYVE domain replicated those of full-length Hrs. Here, neurons in microfluidic chambers were lentivirally transduced with EGFP-2xFYVE, and their dynamic behavior assessed under control, acute bic/4AP, and 2h bic/4AP conditions. Interestingly, while the 2xFYVE domain exhibited highly punctate expression in axons, its dynamics were different from those of full-length Hrs and it did not demonstrate activity-dependent changes in motility (Fig. S4A-F), indicating that other domains of Hrs facilitate its activity-dependent transport. We next assessed whether the FYVE/PI3P interaction was necessary for targeting Hrs to vesicle membranes in neurons. For these experiments, we treated EGFP-Hrs-expressing neurons with an inhibitor of the phosphatidylinositol 3-kinase VPS34, required for synthesis of PI3P (Schu et

al. 1993). Two hours of treatment with the inhibitor (SAR405) dramatically decreased the number of somatodendritic Hrs puncta compared to vehicle control (Fig. 5A, B, D). This effect was replicated by an inactivating mutation of the Hrs FYVE domain (R183A; (Raiborg et al. 2001))(Fig. 5C-D), indicating that the FYVE/PI3P interaction is critical for membrane targeting of Hrs in neurons. However, 2h treatment with SAR405 did not alter the number or motility of axonal Hrs puncta (Fig. 5E-I), suggesting that Hrs association with vesicles occurs in the somatodendritic compartment prior to axonal transport, and remains stable in axons over the course of several hours.

KIF13A mediates the transport of Hrs+ vesicles

Axonal Hrs puncta exhibit pronounced changes in directional motility following 2h bic/4AP treatment, in particular a >two-fold increase in anterograde transport (Fig. 2F). These findings suggest that a plus-end directed kinesin motor protein mediates the activity-dependent transport of Hrs. Previous studies have identified several kinesins responsible for the plus-end directed transport of early endosomes, including the kinesin-3 family members KIF13A and KIF13B (Bentley et al. 2015; Huckaba et al. 2011). Using an assay developed to evaluate the ability of specific kinesins to transport various cargo (Bentley and Banker 2015), we examined whether KIF13A and/or KIF13B mediate the transport of Hrs. We first confirmed the efficacy of this assay in Neuro2a (N2a) cells, by transfecting cells with the minus-end directed motor domain of BicD2 (BicD2-GFP-FKBP) together with the cargo binding domain of KIF13A or KIF13B (KIF13A-FRB-Myc, KIF13B-FRB-Myc). As previously reported, addition of membrane-permeant rapamycin analog to link the FRB and FKBP domains led to the cotransport of BicD2 and KIF13A/B to the cell centrosome (Fig. S5A-B). Moreover, we were able to recapitulate transport of Rab5 by both KIF13A and KIF13B as previously observed (Fig. S5C-F; (Bentley et al. 2015)). We next tested the ability of KIF13A and KIF13B to facilitate transport of RFP-Hrs. Surprisingly, while Hrs was readily transported to the centrosome in the presence of the linker and KIF13A (Fig. 6A-B), it was not transported in the presence of KIF13B (Fig. 6C-D). These findings indicate a specificity of the transport mechanism for Hrs+ vesicles that does not exist for all Rab5+ vesicles. We further tested the specificity of interactions between Hrs and KIF13A/B by coimmunoprecipitation in N2a cells cotransfected with RFP-Hrs, STAM-mCh, or mCherry control, together with the KIF13A- or KIF13B-FRB-Myc constructs. Consistent with our transport assays, we found that Hrs clearly precipitated KIF13A, but not KIF13B (Fig. 6E-F). STAM1 also had some ability to precipitate KIF13A, albeit variably, but did not precipitate KIF13B (Fig. 6E-F).

These findings suggest that Hrs, and potentially STAM1, interact with KIF13A, and identify this motor protein as a candidate for the activity-dependent transport of axonal ESCRT-0 vesicles.

Knockdown of KIF13A inhibits SV protein degradation and activity-dependent Hrs motility

To test whether KIF13A is necessary for the transport of ESCRT-0 vesicles, we examined the effects of KIF13A knockdown on ESCRT-0 protein transport and function. For these studies, we used an shRNA against rat KIF13A (sh13A) that produced a ~60% knockdown of the protein after lentiviral transduction (between 7-14 DIV; Fig. S6A-B). Our previous work showed that Hrs knockdown inhibits the degradation of several SV membrane proteins, including Synaptic Vesicle protein 2 (SV2) and Vesicle-associated membrane protein 2 (VAMP2)(Sheehan et al. 2016). We reasoned that knockdown of KIF13A should similarly impair the degradation of these SV proteins if it is required for axonal transport of Hrs. To test this concept, we used our previously-described cycloheximide-chase assay (Sheehan et al. 2016) to measure the degradation of SV2 and VAMP2 in neurons expressing sh13A or a scrambled control shRNA (shCtrl). We found that both SV2 and VAMP2 degradation were slowed in the presence of sh13A compared to shCtrl (Fig. 7A-C), suggesting that KIF13A is necessary for facilitating degradation of these SV proteins. To examine the effects of KIF13A knockdown on the axonal motility of Hrs, we coexpressed EGFP-Hrs together with sh13A or shCtrl in neurons cultured in microfluidic chambers. Time-lapse imaging revealed that sh13A expression did not alter either the motility, (Fig. 7D,F) directional movement, (Fig. S6C) or speed (Fig. S6D) of Hrs under control conditions compared to shCtrl. However, this hairpin completely abolished the activity-dependent increase in Hrs motility (Fig. 7E-F, Videos 8&9). Similar effects were seen for STAM1, as baseline puncta motility was unaffected by sh13A, while activity-dependent motility was inhibited (Fig. 7G; Fig. S6E-F). Overall, these data indicate that KIF13A is responsible for the activity-dependent transport of ESCRT-0 vesicles in axons.

Discussion

In this study, we demonstrate a novel mechanism for spatiotemporal regulation of the ESCRT pathway in neurons. Our findings show that axonal transport vesicles carrying ESCRT-0 proteins exhibit increased anterograde and bidirectional motility in response to neuronal firing (Fig. 8), providing the first example of activity-dependent transport of degradative machinery in axons. Previous studies have reported that both the axonal motility of mitochondria and the inter-bouton transport of SVs in hippocampal neurons are regulated by neuronal activity,

specifically presynaptic calcium influx (Lin and Sheng 2015; Chen and Sheng 2013; Gramlich and Klyachko 2017; Qu et al. 2019). These processes are hypothesized to contribute to the activity-dependent remodeling of synapses to alter neurotransmitter release properties (Gramlich & Klyachko, 2017, Cell Reports; Lin & Sheng, 2015, Experimental Cell Research). Synaptic activity has also been shown to induce the postsynaptic recruitment of proteasomes and lysosomes in cultured neurons, as well as the local biogenesis of autophagosomes at pre- and postsynaptic sites (Wang et al. 2015; Bingol and Schuman 2006; Goo et al. 2017; Shehata et al. 2012; Soukup et al. 2016; Vanhauwaert et al. 2017; Kulkarni and Maday 2018). However, the axonal transport of autophagosomes in cultured neurons appears to be a constitutive process that is unaffected by stimuli such as synaptic activity and glucose levels (Maday and Holzbaur 2016; Maday, Wallace, and Holzbaur 2012). Axonal autophagosomes, once formed, undergo reliable retrograde trafficking to the soma with their cargo while acidifying into autolysosomes (Maday and Holzbaur 2016; Maday, Wallace, and Holzbaur 2012). In contrast, we find that axonal transport of ESCRT-0 proteins Hrs and STAM1 is bidirectional and highly sensitive to neuronal activity levels. These characteristics likely facilitate increased contact of this early ESCRT machinery with SV pools, thereby catalyzing the activity-dependent degradation of SV proteins.

Our data indicate that axonal ESCRT-0+ vesicles represent a specialized endosomal subtype. Endosomes are highly dynamic and heterogenous structures in all cells, and particularly in neurons, whose complex morphology and high protein trafficking demands have given rise to multiple distinct classes of endosomes that are spatially restricted within different neuronal compartments (Maday and Holzbaur 2016; Yap et al. 2018). Early endosomes are classically defined by the markers Rab5 and EEA1 (Langemeyer, Fröhlich, and Ungermann 2018; Simonsen et al. 1998; Gorvel et al. 1991); however, recent studies have identified sub-categories of early endosomes in neurons that can be differentiated both by their markers and axonal transport patterns (Olenick, Dominguez, and Holzbaur 2018; Leonard et al. 2008). The ESCRT-0 transport vesicles that we describe here represent a new addition to this category. We find that while the total pool of axonal Rab5+ vesicles exhibits high motility under baseline conditions and relatively modest activity-induced increases in anterograde motility, the Hrs+ subset of this pool exhibits limited motility at baseline, but significant activity-induced anterograde and bidirectional motility (Figs 2-4). Moreover, our CLEM experiments demonstrate that Hrs+ vesicles are degradative structures (Fig. S2), though we cannot yet correlate their morphology with their axonal transport history to determine what stage of the degradative process they represent. We did not assess STAM1 vesicle morphology or colocalization with

Rab5 in this study, but we have previously observed that co-expressed Hrs and STAM1 are highly colocalized in axons, and we find here that STAM+ vesicles exhibit very similar activity-dependent dynamics to Hrs+ vesicles (Fig. 3). This unique sensitivity of ESCRT-0 vesicles to neuronal activity, together with their morphological characteristics and ubiquitin-dependent colocalization with SV pools (Fig. S1), suggests to us that they have a specific function: mediating the activity-dependent degradation of old and/or dysfunctional SV proteins. This hypothesis, to be further explored in future studies, aligns with previous research indicating that SV proteins become increasingly dysfunctional as they age and undergo multiple cycles of exo/endocytosis (Truckenbrodt et al. 2018; Fernandes et al. 2014).

In addition to characterizing the dynamic behavior and morphology of ESCRT-0 axonal transport vesicles, this study investigates the mechanisms of Hrs targeting to these vesicles. As in non-neuronal cells (Gaullier et al. 2000; Komada & Soriano 1999), we find that Hrs' association with vesicles is dependent upon interactions between its FYVE domain and the endosomal lipid PI3P (Fig. 5). Blocking PI3P synthesis with a VPS34 inhibitor (SAR405), or expressing a FYVE domain-inactivating mutant form of Hrs, leads to the near-complete loss of Hrs membrane targeting in the somatodendritic compartment (Fig. 5). However, treatment with the SAR405 does not alter the number, speed, or motility of Hrs puncta in axons (Fig. 5). Together, these findings indicate that the axonal pool of Hrs-positive vesicles is assembled in the somatodendritic compartment, and that Hrs interactions with axonal transport vesicles are stable for at least 2 hours. A potential alternative explanation for this finding is that a different domain of Hrs mediates its association with axonal vesicles. Indeed, it was previously reported that the FYVE domain is insufficient for Hrs membrane targeting, as the C-terminal coiled-coil domain is also necessary for this function (Raiborg et al. 2001). Interestingly, the coiled-coil domain of Hrs is known to interact with SNAP-25 (Kwong et al. 2000), a SV-associated protein and component of the SNARE complex required for SV fusion (McMahon & Südhof 1995; Söllner et al. 1993). Given that SNAP-25 must also be transported to presynaptic terminals, it is conceivable that its presence on axonal transport vesicles is required for the recruitment and/or stabilization of Hrs. It is also interesting to note that EEA1, which targets to early endosome membranes via its FYVE domain, does not localize to axons (Gaullier et al. 2000; Lawe et al. 2000; Wilson et al., 2000), indicating that additional domains and protein interactions may be required for axonal targeting of FYVE domain-containing proteins.

Finally, our work has elucidated the mechanism of activity-dependent transport of ESCRT-0+ vesicles, in particular the role of kinesin-3 family member KIF13A in this process. Surprisingly, we find that although both KIF13A and KIF13B mediate transport of Rab5 in a

reconstituted transport assay (Fig. S5), as previously reported (Bentley et al. 2015), only KIF13A transports Hrs (Fig. 6). This specificity is confirmed by coimmunoprecipitation assays in which Hrs precipitates KIF13A but not KIF13B, further bolstering the concept that ESCRT-0 vesicles comprise a specialized subset of pro-degradative endosomes with unique transport properties. KIF13A and KIF13B are highly homologous proteins that share multiple cargoes, including early and recycling endosome associated proteins Rab5, Rab10, and transferrin receptor (Jenkins et al. 2012; Bentley et al. 2015; Etoh & Fukuda 2019). These kinesins also have distinct cargoes, including low density lipoprotein receptor (for KIF13B; Jenkins et al. 2012) and serotonin type 1a receptor (for KIF13A; Zhou et al. 2013), as well as Hrs and STAM1. It is possible that these distinct cargoes reflect differences in the subcellular localization of KIF13A and KIF13B in neurons. However, current reports about their localization are conflicting, with one study showing that KIF13A localizes to axonal and dendritic vesicles while KIF13B is primarily dendritic (Jenkins et al. 2012), and another showing that KIF13B has an axonal bias whereas KIF13A is exclusively dendritic (Yang et al. 2019). In our experiments, we find that knockdown of KIF13A prevents the activity-induced motility of Hrs and STAM1 in axons (Fig. 7), indicating that KIF13A has an essential role in the axonal transport of these ESCRT-0 proteins. Our findings also highlight the importance of KIF13A-mediated transport in SV protein degradation, which is impaired by KIF13A knockdown under basal conditions (Fig. 7). These data suggest that activity-dependent transport of ESCRT-0 proteins occurs even under conditions of lower neuronal firing, but may be difficult to capture during our 4-minute imaging sessions. Additional work is needed to identify the other motor proteins responsible for ESCRT-0 vesicle motility, including the dynein adaptors involved in retrograde transport of these vesicles.

The ESCRT pathway plays a vital role in maintaining neuronal health, and is intimately linked to neurodegenerative disease etiology. Here, we have illuminated a novel mechanism for spatiotemporal regulation of the ESCRT pathway in neurons, based on the activity-induced axonal transport of pro-degradative ESCRT-0 vesicles by kinesin motor protein KIF13A. These findings broaden our understanding of how protein degradation is regulated in neurons, and shed light on how disruption of this degradative pathway may contribute to the etiology of neurodegenerative disease.

Materials and methods

Cell Culture

Hippocampal neurons were prepared from E18 Sprague Dawley rat embryos of both sexes using a modified Banker culture protocol (Kaech & Banker 2006; Sheehan et al., 2016; Waites et al. 2009). Neurons were dissociated in TrypLE Express (ThermoFisher/Invitrogen) for 20min, washed with Hanks Balanced Salt Solution (Sigma), and plated in Neurobasal medium (ThermoFisher/Invitrogen) with N21 supplement (R&D Systems) and Glutamax (ThermoFisher/Invitrogen) at a density of 250,000 neurons per well (12 well plates), coverslip (22 x 22 mm square) or 35mm glass-bottom dish (MatTek), or at a density of 100,000 neurons per microfluidic chamber. Coverslips and dishes were pre-coated with 0.25 mg/mL poly-L-lysine (Sigma-Aldrich) in 100 mM boric acid (pH 8.0) for 24 h before plating. Neuro2a (N2a) neuroblastoma cells (ATCC CCL-131) and HEK293T cells (Sigma) were cultured in DMEM-GlutaMAX (ThermoFisher/Invitrogen) with 10% FBS (Atlanta Biological) and Antibiotic-Antimycotic (ThermoFisher/Invitrogen) and kept at 37°C in 5% CO_2.

Microfluidic Chambers

Microfluidic molds and chambers were prepared as described in (Birdsall et al., 2019). Chambers were prepared by pouring ~30mL of PDMS mixture (QSil 216) into molds, then baking at 70° C overnight.

DNA Constructs

pVenus-2xFYVE was a gift from F. Polleux and was subcloned into pFUGWm vector (Waites et al. 2013) at MfeI/NheI sites; pFU-RFP-Hrs-W, pFU-STAM-mCh-W, pFU-EGFP/mCh-Rab35, and pFU-EGFP/mCh-Rab5 were described in (Sheehan et al. 2016)); pFU-EGFP-Synapsin-W was described in (Leal-Ortiz et al. 2008); and pBa-eGFP-flag-BicD2594-FKBP (Addgene plasmid #63569; http://n2t.net/addgene:63569; RRID:Addgene_63569), pBa-FRB-3myc-KIF13A tail 361-1749 (Addgene plasmid #64288; http://n2t.net/addgene:64288; RRID:Addgene_64288), and pBa-FRB-3myc-KIF13B tail 442-1826 (Addgene plasmid #64289; http://n2t.net/addgene:64289; RRID:Addgene_64289) were gifts from Gary Banker and Marvin Bentley (Jenkins et al. 2012; Bentley et al. 2015; Bentley and Banker 2015). Full-length human Hrs (NCBI accession #D84064.1) was synthesized at Genewiz and cloned into pFUGWm vector at BsrGI/XhoI sites to create pFU-EGFP-Hrs-W, and EGFP replaced with Halotag at the AgeI/BsrGI sites to create pFU-Halo-Hrs-W. To create pFU-EGFP-R183A Hrs-W, an 868 nucleotide fragment of Hrs containing the R183A mutation was synthesized at Genewiz and subcloned into the BsrGI/PshAI sites. shRNA scrambled control and KIF13A knockdown constructs (shCtrl, sh13A) were purchased from Origene (catalog #TL706020). The 29mer

shRNA (lower-case letters) and surrounding loop sequences (capital letters)(shCtrl:CGGATCGgcactaccagagctaactcagatagtactTCAAGAG agtactatctgagttagctctggtagtgcTTTTT; sh13A:CGGATCGagccagacctctatgatagcaaccatcag TCAAGAGctgatggttgctatcatagaggtctggctTTTTTT) were then re-synthesized and subcloned into pFUGW U6 vector (Waites et al. 2013) at EcoRI/PacI sites.

Pharmacological Treatments

Pharmacological agents were used in the following concentrations and time courses: cycloheximide (Calbiochem, 0.2 µg/µl, 24 h), bicuculline (Sigma, 40 µM, 5 min-2h), 4-aminopyridine (Tocris Bioscience, 50 µM, 5 min-2h), AP5 (Tocris Bioscience, 50 µM, 1 h), CNQX (Tocris Bioscience, 10 µM, 1 h), TTX (Tocris Bioscience, 0.5 µM, 2 h), PR-619 (LifeSensors, 50 µM, 2 h), Rapamycin analogue linker drug (AP21967, Clonetech, 100 nM, 3 h), SAR405 (Millipore Sigman, 1 µM, 2h). Unless otherwise indicated, all other chemicals were purchased from Sigma.

Evaluation of Neuronal Health

Cell health in microfluidic chambers was evaluated using NucRed Dead 647 reagent to identify cells with compromised membranes along with membrane-permeant NucBlue™Live ReadyProbes™ Reagent (both ThermoFisher) to evaluate the total number of cells. Neurons were treated with these reagents for 15 min then immediately imaged as described (see Live Neuron Imaging).

Lentiviral Transduction and Neuronal Transfection

Lentivirus was produced using HEK293T cells as previously described (Birdsall et al., 2019; Sheehan et al., 2016). Neurons were transduced with 50-150 µL of lentivirus on 7 DIV, and imaged or fixed on 13-15 DIV. Neurons were transfected as described in (Sheehan et al. 2016) using Lipofectamine 2000 (ThermoFisher/Invitrogen) on 9 DIV. Briefly, for each 22x22 mm coverslip or 35 mm dish, 2.5 µL Lipofectamine was incubated with 62.5 µL Neurobasal for 5 min, combined with 2.5 µg DNA diluted into 62.5 µL Neurobasal for 15 min, then added to neurons for 1 h at 37°C. Neurons were transfected in Neurobasal medium containing 50 µM AP5 and 10 µM CNQX, washed 3X in this medium, and then returned to their original medium following transfection. Lentivirus was fluidically isolated in chambers as previously described (Birdsall et al., 2019). Briefly, ~50% of the media from the wells to be infected was removed and placed in

adjacent wells, then virus was infected into the reduced-volume wells to contain it within those compartments (Fig. S1A).

Electron micrograph analysis of endosomal structures

Electron microscopy of hippocampal synapses was performed by Glebov and Burrone as described (Glebov et al. 2016). Presynapses were defined visually by the presence of synaptic vesicle pools. Endosomal structures were defined as single-membraned structures with a diameter >80nm. Multilamellar structures were defined a structures with more than one visible membrane. Synaptic area and endosomal/multilamellar structure size were measured using FIJI.

Correlative light and electron microscopy methods

For correlative fluorescence and electron microscopy experiments, mouse hippocampal neurons were cultured on sapphire disks (Technotrade #616-100) that were carbon-coated in a grid pattern (using finder grid masks; Leica microsystems, #16770162) to locate the region of interest by electron microscopy. Following 1mg/mL poly-L-lysine (Sigma #P2636) coating overnight, neurons were seeded at densities of 2.5×10^2 cell/mm^2 in 12-well tissue-culture treated plates (Corning #3512) and cultured in NM0 medium (Neurobasal medium (Gibco #21103049) supplemented with 2% B27 plus (Life Technologies # A3582801) and 1% GlutaMAX (Thermo Fischer #35050061). STAM-Halo, HRS-Halo and vGlut1-pHluorin were lentivirally transduced at 6 DIV, and experiments performed at 14-15 DIV. To induce activity, 40 µM bicuculine (Bic)(Tocris #0130/50) and 50 µM 4-aminopyridine (4AP)(Tocris #940) were added to the culture media at 37°. Following 2h incubation, half of the media was changed to NM0 with 2 mM Jenelia-Halo-549 nm (Lavis Lab #SB-Jenelia-Halo-549) and incubated for an additional 30 min at 37°. Neurons on the sapphire disks were washed 3X with PBS, fixed with 4% paraformaldehyde (EMS #15714) and 4% sucrose (Sigma #S0389) in PBS for 20 min at room temperature, washed again 3X with PBS, and mounted on a confocal scanning microscope (Carl Zeiss; LSM880) using a chamber (ALA science #MS-508S). Z-series of fluorescence images were acquired using a 40x objective lens at 2048x2048 pixel resolution. Differential interface contrast images of the carbon grid pattern and neurons on the sapphire disks were also acquired to locate the cells in later steps.

Following fluorescence imaging, neurons were prepared for electron microscopy. Here, sapphire disks were placed into 12-well plate containing 1 mL of 2% glutaraldehyde (EMS #16530) and 1 mM $CaCl_2$ (Sigma-Aldrich # 63535) in 0.1 M sodium cacodylate (Sigma-Aldrich #C0250) pH 7.4, and incubated for 1 h on ice. Subsequently, the sapphire disks were washed

with 1 mL of chilled 1M cacodylate buffer 3X for 5 min each. Neurons were then postfixed for 1 h on ice with 2 mL of 1% osmium tetroxide (EMS #RT19134) and 1% potassium ferrocyanide (Sigma-Aldrich #P3289) in 0.1 M sodium cacodylate, pH 7.4. After washing 3X with 2 mL of water for 5 min, neurons were stained with 1 mL of 2% uranyl acetate (Polysciences #21447-25) in water for 30 min at room temperature and then briefly washed with 50% ethanol (Pharmco #111000200) before dehydration in a graded ethanol series (50%, 70%, 90% for 5 min each, and 100% for 5 min 3x). After dehydration, sapphire disks were embedded into 100% epon-araldite resin (Ted Pella #18005, 18060, 18022) with the following schedule and conditions: overnight at 4 ºC, 6 h at room temperature (solution exchange every 2 h), and 48 h at 60 ºC.

For electron microscopy imaging, regions of interest were located based on the bright field images. When a sapphire disk is removed, neurons and carbon-coating remain in the plastic block, which was trimmed to the regions of interest and sectioned with a diamond knife using an ultramicrotome (Leica; UC7). Approximately 40 consecutive sections (80 nm each) were collected onto the pioloform-coated grids and imaged on a Phillips transmission electron microscope (CM120) equipped with a digital camera (AMT; XR80). The fluorescence and electron micrographs were roughly aligned based on size of the pixels and magnification, and the carbon-coated grid patterns. The alignment was slightly adjusted based on the visible morphological features.

Immunofluorescence Microscopy

Neurons or N2a cells were immunostained as described previously (Leal-Ortiz et al. 2008; Sheehan et al. 2016). Briefly, coverslips were fixed with Lorene's Fix (60 mM PIPES, 25 mM HEPES, 10 mM EGTA, 2 mM $MgCl_2$, 0.12 M sucrose, 4% formaldehyde) for 15 min, incubated with primary and either Alexa-488- or Alexa-647-conjugated secondary antibodies diluted in blocking buffer (2% glycine, 2% BSA, 0.2% gelatin, 50 mM NH_4Cl in PBS) for 1h at room temperature, and washed 4X with PBS between antibody incubations. Coverslips were mounted with DAPI VectaShield (Vector Laboratories) and sealed with clear nail polish. Alternatively, coverslips were mounted with Aqua-Poly/Mount (Polysciences) and dried overnight in the dark. Images were acquired with a 40x objective (Neofluar, NA 1.3) or 63x objective (Neofluar, NA 1.4) on an epifluorescence microscope (Axio Observer Z1, Zeiss) with Colibri LED light source, EMCCD camera (Hamamatsu) and Zen 2012 (blue edition) software. Images were obtained and processed using Zen Blue 2.1 software. Image processing was done using FIJI (Image-J).

In vitro KIF13A/KIF13B transport assay

N2a cells were transfected at 50-70% confluence with BicD2-GFP-FKBP, KIF13A-FRB-Myc or KIF13B-FRB-Myc, and either mCh, mCh-Rab5, or STAM-mCh, using Lipofectamine 3000 (ThermoFisher/Invitrogen) according to manufacturer's instructions. After 48h, rapamycin analogue (AP21967) or EtOH control was added to relevant samples as described in (Bentley and Banker 2015). After 3h of treatment, cells were fixed and imaged as described in **Immunofluorescence Microscopy**.

Live Imaging

Neurons were imaged at 12-15 DIV after being transduced on 7 DIV, or transfected at 9 DIV. Imaging was conducted in pH-maintaining Air Media, consisting of 250 mL L15 Media (ThermoFisher/Invitrogen) and 225 mL Hanks Balanced Salt Solution (Sigma), supplemented with 55mM HEPES, 2% B27 (ThermoFisher), 0.5mM GlutaMAX (ThermoFisher), 0.1% Pen/Strep, 0.5% Glucose, and 2.5% BME. Neurons were imaged at 37°C with a 40x oil-immersion objective (Neofluar, NA 1.3) on an epifluorescence microscope (Axio Observer Z1, Zeiss) with Colibri LED light source, EMCCD camera (Hamamatsu) and Zen 2012 (blue edition) software. One frame was taken every 5 seconds, for a total of 50 frames. Images were obtained and processed using Zen Blue 2.1 software. Axons were identified via location and morphological criteria. Image processing was done using FIJI (Image-J).

Live Imaging Analysis

Motility of axonal puncta was analyzed using FIJI's "Manual Tracker" plugin. Raw data for the movement of each puncta over each video frame were imported into Matlab and motility, directionality, and speed were calculated using a custom program. Only puncta ≥0.5 microns and <1.5 microns in diameter were analyzed. Directionality of each puncta was categorized as follows: ≥4 µm away from the cell body = anterograde, ≥4 µm towards the cell body = retrograde, ≥4 µm total, but <4 µm in one direction = bidirectional, <4 µm = stationary. Axon length was measured in FIJI.

Immunoprecipitation and Western Blot

For immunoprecipitation assays, N2a cells were transfected at 50-70% confluence using Lipofectamine 3000 (ThermoFisher/Invitrogen) according to manufacturer's instructions. Cells were collected 48 h later in lysis buffer (50 mm Tris-Base, 150 mm NaCl, 1% Triton X-100, 0.5% deoxycholic acid) with protease inhibitor mixture (Roche) and clarified by centrifugation at high speed (20,000 rcf). Resulting supernatant was incubated with Dynabeads

(ThermoFisher/Invitrogen) coupled to anti-mCherry antibodies (polyclonal; Biovision). Lysates and beads were incubated at 4°C under constant rotation for 2 h. Beads were washed 2–3X with PBS containing 0.05% Triton (PBST) and then once with PBS. Bound proteins were eluted using sample buffer (Bio-Rad) and subject to SDS-PAGE immunoblotting as described following. For all other immunoblotting experiments, neurons were collected directly in 2X SDS sample buffer (Bio-Rad). Samples were subjected to SDS-PAGE, transferred to nitrocellulose membranes, and probed with primary antibody in 5% BSA/PBS + 0.05% Tween 20 overnight at 4°C, followed by DyLight 680 or 800 anti-rabbit, anti-mouse, or anti-goat secondary antibodies (ThermoFisher) for 1 h. Membranes were imaged using an Odyssey Infrared Imager (model 9120, LI-COR Biosciences). Protein intensity was measured using the “Gels” function in FIJI.

Statistical Analyses

All statistical analyses were performed in GraphPad Prism. Statistics for each experiment are described in the Figure Legends. A D’Agostino-Pearson normality test was used to assess normality. An unpaired Student’s t test or a Mann–Whitney U test was used to compare two datasets, and an ANOVA or a Kruskal-Wallis test was used to compare three or more datasets. For multiple comparisons, Dunnett’s or Dunn’s post-hoc test was used to compare a control mean to other means, while Sidak’s post-hoc test was used to compare pairs of means. Statistical significance is noted as follows (and in Figure Legends): ns, $P>0.05$; *, $P\leq0.05$; **, $P\leq0.01$; ***, $P\leq0.001$. All experiments were repeated with at least 3 independent sets of samples.

Supplemental Material

Supplemental Figures 1-6 and Supplemental Figure legends

Acknowledgements

This work was supported by NIH grants 2R01NS080967 to C.W. and S.W., 5T32NS064928 to V.B., and Hirschl Research Scientist Award to C.W. We would like to thank Drs. Oleg Glebov and Juan Burrone (King’s College, London, UK) for generously sharing EM micrographs of synapses from hippocampal neurons treated with TTX and gabazine, Dr. Ulrich Hengst (Columbia University) and Hengst lab members for help with microfluidic chambers, and members of the Waites lab for their scientific input. The authors declare no competing financial interests.

Author Contributions

V.B. and C.W. designed the research, V.B. and Y.I. performed experiments and analyzed data, C.W. and S. W. supervised the research, and V.B. and C.W. wrote the manuscript.

References

Bentley, Marvin, and Gary Banker. 2015. “A Novel Assay to Identify the Trafficking Proteins That Bind to Specific Vesicle Populations.” *Current Protocols in Cell Biology* 69 (1): 13.8.1-13.8.12. https://doi.org/10.1002/0471143030.cb1308s69.

Bentley, Marvin, Helena Decker, Julie Luisi, and Gary Banker. 2015. “A Novel Assay Reveals Preferential Binding between Rabs, Kinesins, and Specific Endosomal Subpopulations.” *Journal of Cell Biology* 208 (3): 273–81. https://doi.org/10.1083/jcb.201408056.

Bezprozvanny, Ilya, and Peter Robin Hiesinger. 2013. “The Synaptic Maintenance Problem: Membrane Recycling, Ca2+homeostasis and Late Onset Degeneration.” *Molecular Neurodegeneration* 8 (1): 23. https://doi.org/10.1186/1750-1326-8-23.

Bingol, Baris, and Erin M Schuman. 2006. “Activity-Dependent Dynamics and Sequestration of Proteasomes in Dendritic Spines.” *Nature* 441 (7097): 1144–48. https://doi.org/10.1038/nature04769.

Birdsall, Veronica, Jose C Martinez, Lisa Randolph, Ulrich Hengst, and Clarissa L Waites. 2019. *Live Imaging of ESCRT Proteins in Microfluidically Isolated Hippocampal Axons BT - The ESCRT Complexes: Methods and Protocols*. Edited by Emmanuel Culetto and Renaud Legouis. New York, NY: Springer New York. https://doi.org/10.1007/978-1-4939-9492-2_9.

Borland, Helena, and Frederik Vilhardt. 2017. “Prelysosomal Compartments in the Unconventional Secretion of Amyloidogenic Seeds.” *International Journal of Molecular Sciences* . https://doi.org/10.3390/ijms18010227.

Chen, Yanmin, and Zu Hang Sheng. 2013. “Kinesin-1-Syntaphilin Coupling Mediates Activity-Dependent Regulation of Axonal Mitochondrial Transport.” *Journal of Cell Biology*. https://doi.org/10.1083/jcb.201302040.

Christ, Liliane, Camilla Raiborg, Eva M Wenzel, Coen Campsteijn, and Harald Stenmark. 2017. “Cellular Functions and Molecular Mechanisms of the ESCRT Membrane-Scission Machinery.” *Trends in Biochemical Sciences* 42 (1): 42–56. https://doi.org/10.1016/j.tibs.2016.08.016.

Christoforidis, Savvas, Marta Miaczynska, Keith Ashman, Matthias Wilm, Liyun Zhao, Shu-Chin Yip, Michael D Waterfield, Jonathan M Backer, and Marino Zerial. 1999. “Phosphatidylinositol-3-OH Kinases Are Rab5 Effectors.” *Nature Cell Biology* 1 (4): 249–52. https://doi.org/10.1038/12075.

Deinhardt, Katrin, Sara Salinas, Carole Verastegui, Rose Watson, Daniel Worth, Sarah Hanrahan, Cecilia Bucci, and Giampietro Schiavo. 2006. “Rab5 and Rab7 Control Endocytic Sorting along the Axonal Retrograde Transport Pathway.” *Neuron* 52 (2): 293–

305. https://doi.org/10.1016/j.neuron.2006.08.018.

Esposito, Giovanni, Fernandes Ana Clara, and Patrik Verstreken. 2012. “Synaptic Vesicle Trafficking and Parkinson’s Disease.” *Developmental Neurobiology* 72 (1): 134–44. https://doi.org/10.1002/dneu.20916.

Etoh, Kan, and Mitsunori Fukuda. 2019. “Rab10 Regulates Tubular Endosome Formation through KIF13A and KIF13B Motors.” *Journal of Cell Science* 132 (5): jcs226977. https://doi.org/10.1242/jcs.226977.

Feng, Qiong, Yu Luo, Xiang-Nan Zhang, Xi-Fei Yang, Xiao-Yue Hong, Dong-Shen Sun, Xia-Chun Li, et al. 2020. “MAPT/Tau Accumulation Represses Autophagy Flux by Disrupting IST1-Regulated ESCRT-III Complex Formation: A Vicious Cycle in Alzheimer Neurodegeneration.” *Autophagy* 16 (4): 641–58. https://doi.org/10.1080/15548627.2019.1633862.

Fernandes, Ana Clara, Valerie Uytterhoeven, Sabine Kuenen, Yu-Chun Wang, Jan R Slabbaert, Jef Swerts, Jaroslaw Kasprowicz, Stein Aerts, and Patrik Verstreken. 2014. “Reduced Synaptic Vesicle Protein Degradation at Lysosomes Curbs TBC1D24/Sky-Induced Neurodegeneration.” *Journal of Cell Biology* 207 (4): 453–62. https://doi.org/10.1083/jcb.201406026.

Fischer von Mollard, G., B. Stahl, C. Walch-Solimena, K. Takei, L. Daniels, A. Khoklatchev, P. De Camilli, T. C. Sudhof, and R. Jahn. 1994. “Localization of Rab5 to Synaptic Vesicles Identifies Endosomal Intermediate in Synaptic Vesicle Recycling Pathway.” *European Journal of Cell Biology*.

Flores-Rodriguez, Neftali, David A Kenwright, Pei-Hua Chung, Andrew W Harrison, Flavia Stefani, Thomas A Waigh, Victoria J Allan, and Philip G Woodman. 2015. “ESCRT-0 Marks an APPL1-Independent Transit Route for EGFR between the Cell Surface and the EEA1-Positive Early Endosome.” *Journal of Cell Science* 128 (4): 755 LP – 767. https://doi.org/10.1242/jcs.161786.

Gaullier, Jean-Michel, Eva Rønning, David J Gillooly, and Harald Stenmark. 2000. “Interaction of the EEA1 FYVE Finger with Phosphatidylinositol 3-Phosphate and Early Endosomes: ROLE OF CONSERVED RESIDUES .” *Journal of Biological Chemistry* 275 (32): 24595–600. https://doi.org/10.1074/jbc.M906554199.

Glebov, Oleg O, Susan Cox, Lawrence Humphreys, and Juan Burrone. 2016. “Neuronal Activity Controls Transsynaptic Geometry.” *Scientific Reports* 6 (1): 22703. https://doi.org/10.1038/srep22703.

Goo, Marisa S, Laura Sancho, Natalia Slepak, Daniela Boassa, Thomas J Deerinck, Mark H

Ellisman, Brenda L Bloodgood, and Gentry N Patrick. 2017. “Activity-Dependent Trafficking of Lysosomes in Dendrites and Dendritic Spines.” *Journal of Cell Biology* 216 (8): 2499–2513. https://doi.org/10.1083/jcb.201704068.

Gorvel, Jean-Pierre, Philippe Chavrier, Marino Zerial, and Jean Gruenberg. 1991. “Rab5 Controls Early Endosome Fusion in Vitro.” *Cell* 64 (5): 915–25. https://doi.org/10.1016/0092-8674(91)90316-Q.

Goto-Silva, Livia, Marisa P McShane, Sara Salinas, Yannis Kalaidzidis, Giampietro Schiavo, and Marino Zerial. 2019. “Retrograde Transport of Akt by a Neuronal Rab5-APPL1 Endosome.” *Scientific Reports* 9 (1): 2433. https://doi.org/10.1038/s41598-019-38637-0.

Gramlich, Michael W, and Vitaly A Klyachko. 2017. “Actin/Myosin-V- and Activity-Dependent Inter-Synaptic Vesicle Exchange in Central Neurons.” *Cell Reports* 18 (9): 2096–2104. https://doi.org/10.1016/j.celrep.2017.02.010.

Hall, Emma A, Michael S Nahorski, Lyndsay M Murray, Ranad Shaheen, Emma Perkins, Kosala N Dissanayake, Yosua Kristaryanto, et al. 2017. “PLAA Mutations Cause a Lethal Infantile Epileptic Encephalopathy by Disrupting Ubiquitin-Mediated Endolysosomal Degradation of Synaptic Proteins.” *American Journal of Human Genetics* 100 (5): 706–24. https://doi.org/10.1016/j.ajhg.2017.03.008.

Hayakawa, Akira, and Naomi Kitamura. 2000. “Early Endosomal Localization of Hrs Requires a Sequence within the Proline- and Glutamine-Rich Region but Not the FYVE Finger.” *Journal of Biological Chemistry* 275 (38): 29636–42. https://doi.org/10.1074/jbc.M002696200.

Huckaba, Thomas M, Arne Gennerich, James E Wilhelm, Athar H Chishti, and Ronald D Vale. 2011. “Kinesin-73 Is a Processive Motor That Localizes to Rab5-Containing Organelles.” *Journal of Biological Chemistry* 286 (9): 7457–67. https://doi.org/10.1074/jbc.M110.167023.

Hurley, James H. 2015. “ESCRTs Are Everywhere.” *The EMBO Journal* 34 (19): 2398–2407. https://doi.org/10.15252/embj.201592484.

Jenkins, Brian, Helena Decker, Marvin Bentley, Julie Luisi, and Gary Banker. 2012. “A Novel Split Kinesin Assay Identifies Motor Proteins That Interact with Distinct Vesicle Populations.” *Journal of Cell Biology* 198 (4): 749–61. https://doi.org/10.1083/jcb.201205070.

Jimenez, Ana Joaquina, Paolo Maiuri, Julie Lafaurie-Janvore, Séverine Divoux, Matthieu Piel, and Franck Perez. 2014. “ESCRT Machinery Is Required for Plasma Membrane Repair.” *Science* 343 (6174): 1247136. https://doi.org/10.1126/science.1247136.

Kaech, Stefanie, and Gary Banker. 2006. “Culturing Hippocampal Neurons.” *Nature Protocols* 1 (5): 2406–15. https://doi.org/10.1038/nprot.2006.356.

Komada, Masayuki, and Philippe Soriano. 1999. “Hrs, a FYVE Finger Protein Localized to Early Endosomes, Is Implicated in Vesicular Traffic and Required for Ventral Folding Morphogenesis.” *Genes & Development* 13 (11): 1475–85. http://genesdev.cshlp.org/content/13/11/1475.abstract.

Kulkarni, Vineet Vinay, and Sandra Maday. 2018. “Compartment-Specific Dynamics and Functions of Autophagy in Neurons.” *Developmental Neurobiology* 78 (3): 298–310. https://doi.org/10.1002/dneu.22562.

Kwong, J, F L Roundabush, P Hutton Moore, M Montague, W Oldham, Y Li, L S Chin, and L Li. 2000. “Hrs Interacts with SNAP-25 and Regulates Ca(2+)-Dependent Exocytosis.” *Journal of Cell Science* 113 (12): 2273 LP – 2284. http://jcs.biologists.org/content/113/12/2273.abstract.

Langemeyer, Lars, Florian Fröhlich, and Christian Ungermann. 2018. “Rab GTPase Function in Endosome and Lysosome Biogenesis.” *Trends in Cell Biology* 28 (11): 957–70. https://doi.org/10.1016/j.tcb.2018.06.007.

Lawe, Deirdre C, Varsha Patki, Robin Heller-Harrison, David Lambright, and Silvia Corvera. 2000. “The FYVE Domain of Early Endosome Antigen 1 Is Required for Both Phosphatidylinositol 3-Phosphate and Rab5 Binding: CRITICAL ROLE OF THIS DUAL INTERACTION FOR ENDOSOMAL LOCALIZATION .” *Journal of Biological Chemistry* 275 (5): 3699–3705. https://doi.org/10.1074/jbc.275.5.3699.

Leal-Ortiz, Sergio, Clarissa L Waites, Ryan Terry-Lorenzo, Pedro Zamorano, Eckart D Gundelfinger, and Craig C Garner. 2008. “Piccolo Modulation of Synapsin1a Dynamics Regulates Synaptic Vesicle Exocytosis .” *The Journal of Cell Biology* 181 (5): 831–46. https://doi.org/10.1083/jcb.200711167.

Lee, DaWon, Xiaoyue Zheng, Kay Shigemori, Christopher Krasniak, Jie Bin Liu, Chao Tang, Joshua Kavaler, and S Tariq Ahmad. 2019. “Expression of Mutant CHMP2B Linked to Neurodegeneration in Humans Disrupts Circadian Rhythms in Drosophila.” *FASEB BioAdvances* 1 (8): 511–20. https://doi.org/10.1096/fba.2019-00042.

Lee, Jin A., Anne Beigneux, S. Tariq Ahmad, Stephen G. Young, and Fen Biao Gao. 2007. “ESCRT-III Dysfunction Causes Autophagosome Accumulation and Neurodegeneration.” *Current Biology*. https://doi.org/10.1016/j.cub.2007.07.029.

Leonard, Deborah, Akira Hayakawa, Deirdre Lawe, David Lambright, Karl D Bellve, Clive Standley, Lawrence M Lifshitz, Kevin E Fogarty, and Silvia Corvera. 2008. “Sorting of EGF and Transferrin at the Plasma Membrane and by Cargo-Specific Signaling to EEA1-Enriched Endosomes.” *Journal of Cell Science* 121 (20): 3445.

http://jcs.biologists.org/content/121/20/3445.abstract.

Lin, Mei-Yao, and Zu-Hang Sheng. 2015. “Regulation of Mitochondrial Transport in Neurons.” *Experimental Cell Research* 334 (1): 35–44. https://doi.org/https://doi.org/10.1016/j.yexcr.2015.01.004.

Maday, Sandra, and Erika L F Holzbaur. 2016. “Compartment-Specific Regulation of Autophagy in Primary Neurons.” *The Journal of Neuroscience* 36 (22): 5933. http://www.jneurosci.org/content/36/22/5933.abstract.

Maday, Sandra, Karen E Wallace, and Erika L F Holzbaur. 2012. “Autophagosomes Initiate Distally and Mature during Transport toward the Cell Soma in Primary Neurons.” *Journal of Cell Biology* 196 (4): 407–17. https://doi.org/10.1083/jcb.201106120.

Mayers, Jonathan R, Ian Fyfe, Amber L Schuh, Edwin R Chapman, J Michael Edwardson, and Anjon Audhya. 2011. “ESCRT-0 Assembles as a Heterotetrameric Complex on Membranes and Binds Multiple Ubiquitinylated Cargoes Simultaneously.” *Journal of Biological Chemistry* 286 (11): 9636–45. https://doi.org/10.1074/jbc.M110.185363.

McCullough, John, Adam Frost, and Wesley I Sundquist. 2018. “Structures, Functions, and Dynamics of ESCRT-III/Vps4 Membrane Remodeling and Fission Complexes.” *Annual Review of Cell and Developmental Biology* 34 (1): 85–109. https://doi.org/10.1146/annurev-cellbio-100616-060600.

McMahon, Harvey T, and Thomas C Südhof. 1995. “Synaptic Core Complex of Synaptobrevin, Syntaxin, and SNAP25 Forms High Affinity -SNAP Binding Site .” *Journal of Biological Chemistry* 270 (5): 2213–17. https://doi.org/10.1074/jbc.270.5.2213 .

Olenick, Mara A, Roberto Dominguez, and Erika L F Holzbaur. 2018. “Dynein Activator Hook1 Is Required for Trafficking of BDNF-Signaling Endosomes in Neurons.” *The Journal of Cell Biology* 218 (1): 220–33. https://doi.org/10.1083/jcb.201805016.

Parkinson, N., P. G. Ince, M. O. Smith, R. Highley, G. Skibinski, P. M. Andersen, K. E. Morrison, et al. 2006. “ALS Phenotypes with Mutations in CHMP2B (Charged Multivesicular Body Protein 2B).” *Neurology*. https://doi.org/10.1212/01.wnl.0000231510.89311.8b.

Poteryaev, Dmitry, Sunando Datta, Karin Ackema, Marino Zerial, and Anne Spang. 2010. “Identification of the Switch in Early-to-Late Endosome Transition.” *Cell* 141 (3): 497–508. https://doi.org/10.1016/j.cell.2010.03.011.

Qu, Xiaoyi, Atul Kumar, Heike Blockus, Clarissa Waites, and Francesca Bartolini. 2019. “Activity-Dependent Nucleation of Dynamic Microtubules at Presynaptic Boutons Controls Neurotransmission.” *Current Biology* 29 (24): 4231-4240.e5. https://doi.org/10.1016/j.cub.2019.10.049.

Raiborg, Camilla, Bjørn Bremnes, Anja Mehlum, David J Gillooly, Antonello D'Arrigo, Espen Stang, and Harald Stenmark. 2001. "FYVE and Coiled-Coil Domains Determine the Specific Localisation of Hrs to Early Endosomes." *Journal of Cell Science* 114 (12): 2255 LP – 2263. http://jcs.biologists.org/content/114/12/2255.abstract.

Raiborg, Camilla, Tor Erik Rusten, and Harald Stenmark. 2003. "Protein Sorting into Multivesicular Endosomes." *Current Opinion in Cell Biology* 15 (4): 446–55. https://doi.org/https://doi.org/10.1016/S0955-0674(03)00080-2.

Schu, P V, K Takegawa, M J Fry, J H Stack, M D Waterfield, and S D Emr. 1993. "Phosphatidylinositol 3-Kinase Encoded by Yeast VPS34 Gene Essential for Protein Sorting." *Science* 260 (5104): 88 LP – 91. https://doi.org/10.1126/science.8385367.

Sheehan, Patricia, Mei Zhu, Anne Beskow, Cyndel Vollmer, and Clarissa L Waites. 2016. "Activity-Dependent Degradation of Synaptic Vesicle Proteins Requires Rab35 and the ESCRT Pathway." *The Journal of Neuroscience* 36 (33): 8668. http://www.jneurosci.org/content/36/33/8668.abstract.

Shehata, Mohammad, Hiroyuki Matsumura, Reiko Okubo-Suzuki, Noriaki Ohkawa, and Kaoru Inokuchi. 2012. "Neuronal Stimulation Induces Autophagy in Hippocampal Neurons That Is Involved in AMPA Receptor Degradation after Chemical Long-Term Depression." *The Journal of Neuroscience* 32 (30): 10413 LP – 10422. https://doi.org/10.1523/JNEUROSCI.4533-11.2012.

Shimizu, Hideyuki, Satoru Kawamura, and Koichi Ozaki. 2003. "An Essential Role of Rab5 in Uniformity of Synaptic Vesicle Size." *Journal of Cell Science* 116 (17): 3583 LP – 3590. https://doi.org/10.1242/jcs.00676.

Simonsen, Anne, Roger Lippe, Savvas Christoforidis, Jean-Michel Gaullier, Andreas Brech, Judy Callaghan, Ban-Hock Toh, Carol Murphy, Marino Zerial, and Harald Stenmark. 1998. "EEA1 Links PI(3)K Function to Rab5 Regulation of Endosome Fusion." *Nature* 394 (6692): 494–98. https://doi.org/10.1038/28879.

Skibinski, Gaia, Nicholas J. Parkinson, Jeremy M. Brown, Lisa Chakrabarti, Sarah L. Lloyd, Holger Hummerich, Jørgen E. Nielsen, et al. 2005. "Mutations in the Endosomal ESCRTIII-Complex Subunit CHMP2B in Frontotemporal Dementia." *Nature Genetics*. https://doi.org/10.1038/ng1609.

Söllner, Thomas, Sidney W Whiteheart, Michael Brunner, Hediye Erdjument-Bromage, Scott Geromanos, Paul Tempst, and James E Rothman. 1993. "SNAP Receptors Implicated in Vesicle Targeting and Fusion." *Nature* 362 (6418): 318–24. https://doi.org/10.1038/362318a0.

Soukup, Sandra-Fausia, Sabine Kuenen, Roeland Vanhauwaert, Julia Manetsberger, Sergio Hernández-Díaz, Jef Swerts, Nils Schoovaerts, et al. 2016. “A LRRK2-Dependent EndophilinA Phosphoswitch Is Critical for Macroautophagy at Presynaptic Terminals.” *Neuron* 92 (4): 829–44. https://doi.org/https://doi.org/10.1016/j.neuron.2016.09.037.

Spencer, Brian, Sharareh Emadi, Paula Desplats, Simona Eleuteri, Sarah Michael, Kori Kosberg, Jay Shen, et al. 2014. “ESCRT-Mediated Uptake and Degradation of Brain-Targeted α-Synuclein Single Chain Antibody Attenuates Neuronal Degeneration In Vivo</Em>.” *Molecular Therapy* 22 (10): 1753–67. https://doi.org/10.1038/mt.2014.129.

Spencer, Brian, Changyoun Kim, Tania Gonzalez, Alejandro Bisquertt, Christina Patrick, Edward Rockenstein, Anthony Adame, Seung-Jae Lee, Paula Desplats, and Eliezer Masliah. 2016. “α-Synuclein Interferes with the ESCRT-III Complex Contributing to the Pathogenesis of Lewy Body Disease.” *Human Molecular Genetics* 25 (6): 1100–1115. https://doi.org/10.1093/hmg/ddv633.

Stahelin, Robert V, Fei Long, Karthikeyan Diraviyam, Karol S Bruzik, Diana Murray, and Wonhwa Cho. 2002. “Phosphatidylinositol 3-Phosphate Induces the Membrane Penetration of the FYVE Domains of Vps27p and Hrs.” *Journal of Biological Chemistry* 277 (29): 26379–88. https://doi.org/10.1074/jbc.M201106200.

Stoten, Caroline Louise, and Jeremy Graham Carlton. 2018. “ESCRT-Dependent Control of Membrane Remodelling during Cell Division.” *Seminars in Cell & Developmental Biology* 74: 50–65. https://doi.org/https://doi.org/10.1016/j.semcdb.2017.08.035.

Sun, Wei, Qing Yan, Thomas A Vida, and Andrew J Bean. 2003. “Hrs Regulates Early Endosome Fusion by Inhibiting Formation of an Endosomal SNARE Complex .” *The Journal of Cell Biology* 162 (1): 125–37. https://doi.org/10.1083/jcb.200302083.

Takahashi, Hirohide, Jonathan R Mayers, Lei Wang, J Michael Edwardson, and Anjon Audhya. 2015. “Hrs and STAM Function Synergistically to Bind Ubiquitin-Modified Cargoes in Vitro.” *Biophysical Journal* 108 (1): 76–84. https://doi.org/10.1016/j.bpj.2014.11.004.

Tamai, Keiichi, Masafumi Toyoshima, Nobuyuki Tanaka, Noriko Yamamoto, Yuji Owada, Hiroshi Kiyonari, Kazuko Murata, et al. 2008. “Loss of Hrs in the Central Nervous System Causes Accumulation of Ubiquitinated Proteins and Neurodegeneration.” *The American Journal of Pathology* 173 (6): 1806–17. https://doi.org/http://doi.org/10.2353/ajpath.2008.080684.

Truckenbrodt, Sven, Abhiyan Viplav, Sebastian Jähne, Angela Vogts, Annette Denker, Hanna Wildhagen, Eugenio F Fornasiero, and Silvio O Rizzoli. 2018. “Newly Produced Synaptic

Vesicle Proteins Are Preferentially Used in Synaptic Transmission." *The EMBO Journal* 37 (15): e98044. https://doi.org/10.15252/embj.201798044.

Uytterhoeven, Valerie, Sabine Kuenen, Jaroslaw Kasprowicz, Katarzyna Miskiewicz, and Patrik Verstreken. 2011. "Loss of Skywalker Reveals Synaptic Endosomes as Sorting Stations for Synaptic Vesicle Proteins." *Cell* 145 (1): 117–32. https://doi.org/10.1016/j.cell.2011.02.039.

Vagnozzi, Alana N, and Domenico Praticò. 2019. "Endosomal Sorting and Trafficking, the Retromer Complex and Neurodegeneration." *Molecular Psychiatry* 24 (6): 857–68. https://doi.org/10.1038/s41380-018-0221-3.

Vanhauwaert, Roeland, Sabine Kuenen, Roy Masius, Adekunle Bademosi, Julia Manetsberger, Nils Schoovaerts, Laura Bounti, et al. 2017. "The SAC1 Domain in Synaptojanin Is Required for Autophagosome Maturation at Presynaptic Terminals." *The EMBO Journal* 36 (10): 1392–1411. https://doi.org/10.15252/embj.201695773.

Vaz-Silva, João, Patrícia Gomes, Qi Jin, Mei Zhu, Viktoriya Zhuravleva, Sebastian Quintremil, Torcato Meira, et al. 2018. "Endolysosomal Degradation of Tau and Its Role in Glucocorticoid-Driven Hippocampal Malfunction." *The EMBO Journal* 37 (20): e99084. https://doi.org/10.15252/embj.201899084.

Waites, Clarissa L, Sergio A Leal-Ortiz, Nathan Okerlund, Hannah Dalke, Anna Fejtova, Wilko D Altrock, Eckart D Gundelfinger, and Craig C Garner. 2013. "Bassoon and Piccolo Maintain Synapse Integrity by Regulating Protein Ubiquitination and Degradation." *The EMBO Journal* 32 (7): 954–69. https://doi.org/10.1038/emboj.2013.27.

Waites, Clarissa L, Christian G Specht, Kai Härtel, Sergio Leal-Ortiz, David Genoux, Dong Li, Renaldo C Drisdel, et al. 2009. "Synaptic SAP97 Isoforms Regulate AMPA Receptor Dynamics and Access to Presynaptic Glutamate." *The Journal of Neuroscience : The Official Journal of the Society for Neuroscience* 29 (14): 4332–45. https://doi.org/10.1523/JNEUROSCI.4431-08.2009.

Wang, Tong, Sally Martin, Andreas Papadopulos, Callista B Harper, Timur A Mavlyutov, Dhevahi Niranjan, Nick R Glass, et al. 2015. "Control of Autophagosome Axonal Retrograde Flux by Presynaptic Activity Unveiled Using Botulinum Neurotoxin Type A." *The Journal of Neuroscience* 35 (15): 6179 LP – 6194. https://doi.org/10.1523/JNEUROSCI.3757-14.2015.

Wilson, Jean M, Meltsje de Hoop, Natasha Zorzi, Ban-Hock Toh, Carlos G Dotti, and Robert G Parton. 2000. "EEA1, a Tethering Protein of the Early Sorting Endosome, Shows a Polarized Distribution in Hippocampal Neurons, Epithelial Cells, and Fibroblasts." *Molecular Biology of the Cell* 11 (8): 2657–71. https://doi.org/10.1091/mbc.11.8.2657.

Yap, Chan Choo, Laura Digilio, Lloyd P McMahon, A Denise R Garcia, and Bettina Winckler. 2018. “Degradation of Dendritic Cargos Requires Rab7-Dependent Transport to Somatic Lysosomes.” *Journal of Cell Biology* 217 (9): 3141–59. https://doi.org/10.1083/jcb.201711039.

Zhang, Kai, Rotem Fishel Ben Kenan, Yasuko Osakada, Wei Xu, Rachel S Sinit, Liang Chen, Xiaobei Zhao, Jia-Yun Chen, Bianxiao Cui, and Chengbiao Wu. 2013. “Defective Axonal Transport of Rab7 GTPase Results in Dysregulated Trophic Signaling.” *The Journal of Neuroscience* 33 (17): 7451 LP – 7462. https://doi.org/10.1523/JNEUROSCI.4322-12.2013.

Zhou, Ruyun, Shinsuke Niwa, Laurent Guillaud, Ying Tong, and Nobutaka Hirokawa. 2013. “A Molecular Motor, KIF13A, Controls Anxiety by Transporting the Serotonin Type 1A Receptor.” *Cell Reports* 3 (2): 509–19. https://doi.org/10.1016/j.celrep.2013.01.014.

Abbreviations

ESCRT, endosomal sorting complex required for transport

Hrs, hepatocyte growth factor-regulated tyrosine kinase substrate

MVB, multivesicular body

STAM1, signal transducing adaptor molecule 1

SV, synaptic vesicle

Figure Legends

Figure 1. Neuronal activity increases the number of presynaptic endosomes. (A-B) Representative electron micrographs of endosomal structures (single-membrane, >80nm diameter, red arrows; A) and multilamellar structures (>1 membrane, red arrows; B) present at presynaptic boutons from 16-21 DIV hippocampal neurons treated for 48h with TTX or gabazine. Size bar, 500 nm. **(C-D)** Quantification of endosomal structures **(C)** and multilamellar structures **(D)** per μm^2 of presynaptic area at TTX- or gabazine-treated boutons. The density of endosomal structures, but not multilamellar structures, is significantly increased following gabazine treatment. Scatter plot shows median and interquartile range (**** P<0.0001, Mann-Whitney test; n=102 (TTX-treated) and 106 (gabazine-treated) boutons/condition).

Figure 2. Neuronal activity stimulates the transport of Hrs+ vesicles in axons. **(A-C)** Representative images and corresponding kymographs of microfluidically isolated axons from 13-15 DIV hippocampal neurons transduced with RFP-Hrs, under control conditions (A, Video 1), acute treatment with Bicuculline/4AP (B), and 2h treatment with Bicuculline/4AP (C, Video 2). Size bar, 10µm. **(D)** Percentage of motile Hrs puncta in axons, showing a significant increase with acute and 2h Bic/4AP treatment (****P<0.0001, *P<0.05; one-way ANOVA with Dunnett's multiple comparisons test; ≥3 weeks of replicates, n=20 (control), 15 (acute Bic/4AP), 16 (2h Bic/4AP) videos/condition). **(E)** Average speed of motile Hrs puncta (µm/sec), showing no change across conditions. Same 'n' values as D. **(F)** Breakdown of directional movement of Hrs puncta, expressed as percentage of total Hrs puncta. Anterograde and bidirectional movement are significantly increased following 2h Bic/4AP treatment (****P<0.0001, ***P<0.001, **P<0.01, one-way ANOVA with Dunnett's multiple comparisons test; same 'n' values as D). **(G)** Percentage of time that motile Hrs puncta are colocalized with Synapsin puncta during the 4 min imaging session, which does not change across conditions (P>0.05, one-way ANOVA with Dunnett's multiple comparisons test; ≥3 weeks of replicates, n=18 (control), 28 (acute Bic/4AP), 28 (2h Bic/4AP) videos/condition). **(H)** Representative images and corresponding kymographs for hippocampal axons expressing RFP-Hrs and EGFP-Synapsin (Video 3). Arrows show Hrs puncta that colocalize with Synapsin. Size bar, 10µm. All scatter plots show mean ± SEM.

Video 1. Hrs puncta are primarily stationary in axons isolated in microfluidic chambers. RFP-Hrs puncta, soma to the right. All videos obtained using time-lapse epifluorescence microscopy with one frame every 5 seconds. Playback is 5x real time. Still image from video is in Fig. 2A.

Video 2. Neuronal firing increases motility of Hrs in axons isolated in microfluidic chambers. RFP-Hrs puncta, soma to the right. One frame every 5 seconds, playback is 5x real time. Still image from video is in Fig. 2C.

Video 3. Motile Hrs interacts with stationary Synapsin in axons in mass neuronal culture. Red puncta are RFP-Hrs, green puncta are EGFP-Synapsin, soma to the right. One frame every 5 seconds, playback is 5x real time. Still images from video are in Fig. 2H.

Figure 3. Neuronal activity differentially affects the axonal motility of STAM1 and Rab5. (A-C) Representative images and corresponding kymographs of microfluidically isolated axons from 13-15 DIV hippocampal neurons transduced with mCh-STAM1, under control (A, Video 4), acute Bic/4AP (B), and 2h Bic/4AP (C, Video 5) conditions. Size bar, 10µm. **(D)** Percentage of motile STAM1 puncta in axons, showing a significant increase with acute and 2h Bic/4AP treatment (****P<0.0001,**P<0.01, *P<0.05, one-way ANOVA with Dunnett's multiple comparisons test; ≥3 weeks of replicates, n=32 (control), 36 (acute Bic/4AP), 13 (2h Bic/4AP) videos/condition). **(E)** Average speed of motile STAM1 puncta (µm/sec), showing no change across conditions. Same 'n' values as D. **(F-H)** Representative images and corresponding kymographs of microfluidically isolated axons from 13-15 DIV hippocampal neurons transduced with EGFP-Rab5, under control (F, Video 6), acute Bic/4AP (G), and 2h Bic/4AP (H, Video 7) conditions. Size bar, 10µm. **(I)** Percentage of motile Rab5 puncta in axons, showing a significant increase only after 2h Bic/4AP treatment (**P<0.01, Kruskal-Wallis test with Dunn's multiple comparisons test; ≥3 weeks of replicates, n=31 (control), 30 (acute Bic/4AP), 14 (2h Bic/4AP) videos/condition). **(J)** Average speed of motile Rab5 puncta (µm/sec) is unchanged across conditions, as with Hrs and STAM1. Same 'n' values as I. **(K)** Breakdown of directional movement of STAM1 puncta, showing that anterograde, retrograde, and bidirectional movement are all significantly increased following 2h Bic/4AP treatment (****P<0.0001, ***P<0.001, **P<0.01, *P<0.05, one-way ANOVA with Dunnett's multiple comparisons test; same 'n' values as D). **(L)** Breakdown of directional Rab5 puncta movement, showing that only anterograde movement is significantly increased following 2h Bic/4AP treatment (**P<0.01, *P<0.05, one-way ANOVA with Dunnett's multiple comparisons test; same 'n' values as I). All scatter plots and bar graphs show mean ± SEM.

Video 4. STAM motility is similar to that of Hrs in microfluidically-isolated axons under baseline conditions. STAM-mCh puncta, soma to the right. One frame every 5 seconds, playback is 5x real time. Still image from video is in Fig. 3A.

Video 5. STAM motility is similar to that of Hrs in microfluidically-isolated axons under Bic/4AP conditions. STAM-mCh puncta, soma to the right. One frame every 5 seconds, playback is 5x real time. Still image from video is in Fig. 3C.

Video 6. Rab5 is more motile than Hrs at baseline in microfluidically-isolated axons. EGFP-Rab5 puncta, soma to the right. One frame every 5 seconds, playback is 5x real time. Still image from video is in Fig. 3F.

Video 7. Rab5 shows increased motility after 2h Bic/4AP treatment in microfluidically-isolated axons. EGFP-Rab5 puncta, soma to the right. One frame every 5 seconds, playback is 5x real time. Still image from video is in Fig. 3H.

Figure 4. Hrs is present on a subset of Rab5+ vesicles in axons. (A) Representative images and corresponding kymographs for 13-15 DIV hippocampal axons cotransfected with RFP-Hrs and EGFP-Rab5. Arrows show puncta that are positive for both proteins. Size bar, 10µm. **(B)** Percentage of stationary Hrs puncta that are also positive for Rab5, demonstrating no significant difference across conditions ($P>0.05$, one-way ANOVA with Dunnett's multiple comparisons test; ≥3 weeks of replicates, n=14 (control), 18 (acute Bic/4AP), 12 (2h Bic/4AP) videos/condition). **(C)** Percentage of stationary Rab5 puncta that are also positive for Hrs, demonstrating no significant differences across condition. Same ‘n’ values as B. **(D)** Percent of stationary puncta that are positive for both Hrs and Rab5 per 100µm of axon, showing no significant differences across conditions. Same ‘n’ values as B. **(E)** Percentage of motile Hrs puncta that are positive for Rab5, showing a significant increase in motility after 2h of Bic/4AP treatment (*$P<0.05$, Kruskal-Wallis test with Dunn’s multiple comparisons test; same ‘n’ values as B). **(F)** Percentage of motile Rab5 puncta that are also positive for Hrs, showing no significant difference in motility across conditions. Same ‘n’ values as B. **(G)** Percentage of motile puncta that are positive for both Hrs and Rab5 per 100 µm of axon, showing a significance increase in motility after 2h of Bic/4AP treatment (**$P<0.01$, one-way ANOVA with Dunnett's multiple comparisons test; same ‘n’ values as B). All scatter plots show mean ± SEM.

Figure 5. Hrs vesicle association requires FYVE domain/PI3P interactions and occurs in the somatodendritic compartment. (A-C) Representative images of EGFP-Hrs localization in cell bodies and dendrites of 13-15 DIV hippocampal neurons under control conditions (A), after 2h of SAR405 treatment (B), and with the R183A FYVE domain inactivating mutation (C). **(D)** Number of Hrs puncta/μm^2 in the somatodendritic compartment under these conditions, demonstrating significant decreases in puncta density with SAR405 treatment or R183A mutation (***P<0.001, *P<0.05, one-way ANOVA with Dunnett's multiple comparisons test; ≥3 weeks of replicates, n=33 (control), 35 (2h SAR405), 17 (FYVE mutant) images/condition). **(E-F)** Representative images and corresponding kymographs of microfluidically isolated hippocampal axons transduced with EGFP-Hrs, under control conditions (E) and after 2h of treatment with SAR405 (F). **(G)** Number of total Hrs puncta per 100 µm of axon, showing no significant difference across these conditions (P>0.05, unpaired t-test; ≥3 weeks of replicates, n=11 (control), 10 (2h SAR405) videos/condition). **(H)** Average speed of motile Hrs puncta (µm/sec), showing no difference following SAR405 treatment. Same 'n' values as B. **(I)** Percentage of motile Hrs puncta in axons, showing no difference following SAR405 treatment. Same 'n' values as B. All scatter plots show mean ± SEM.

Figure 6. KIF13A, but not KIF13B, mediates transport of Hrs+ vesicles. (A) Representative images of N2a cells co-transfected with RFP-Hrs (red), BicD2-GFP-FKBP (green), and KIF13A-FRB-Myc (blue), +/- rapamycin analogue to link FKBP/FRB (linker). **(B)** Line scan graphs of the images in panel A, showing that addition of the linker induces colocalization of these proteins as depicted by a single peak in the lower graph. **(C-D)** Representative images of N2a cells co-transfected with RFP-Hrs (red), BicD2-GFP-FKBP (green), and KIF13B-FRB-Myc (blue), +/- linker (C), and corresponding line scan graphs (D) showing that addition of linker does not induce protein colocalization. **(E)** Immunoblot of lysates from N2a cells expressing mCh, mCh-STAM, or RFP-Hrs, together with KIF13A-FRB-Myc or KIF13B-FRB-Myc, immunoprecipitated (IP) with mCh antibody and probed with Myc or mCh antibodies. **(F)** Quantitative analysis of KIF13A/B-FRB-Myc band intensity after immunoprecipitation with Hrs or STAM, expressed as intensity normalized to mCh control. Hrs consistently precipitates KIF13A but not KIF13B (**P<0.001, one-way ANOVA with Dunnett's multiple comparisons test; ≥3 weeks of replicates). Bars show mean ± SEM.

Figure 7. Knockdown of KIF13A inhibits SV protein degradation and activity-dependent Hrs transport. (A) Representative immunoblots of SV2 and VAMP2, with corresponding tubulin

loading controls, from lysates of 14 DIV hippocampal neurons transduced with shCtrl or sh13A to knockdown KIF13A, and treated for 24h with DMSO control (CON) or cycloheximide (CHX). **(B-C)** Quantification of the fold-change in SV2 (C) and VAMP2 (D) degradation under these conditions, calculated as previously described (Sheehan et al. 2016). Degradation of both proteins is significantly decreased in the presence of sh13A (*P<0.05, unpaired t-test; ≥3 weeks of replicates, n=5 (SV2), 11 (VAMP2) cell lysates/condition). **(D)** Representative images and corresponding kymographs of microfluidically isolated hippocampal axons transduced with EGFP-Hrs and shCtrl under control conditions (upper panels) and after 2h treatment with Bic/4AP (lower panels, Videos 8&9). Size bar, 10µm. **(E)** Representative images and corresponding kymographs of microfluidically isolated hippocampal axons expressing EGFP-Hrs and sh13A under control conditions (upper panels) and after 2h treatment with Bic/4AP (lower panels). Size bar, 10µm. **(F)** Percentage of motile Hrs puncta in axons, showing that the increased motility of Hrs after 2h Bic/4AP treatment is abolished in sh13A-expressing neurons (***P<0.001, one-way ANOVA with Sidak's multiple comparisons test; ≥3 weeks of replicates, n=14 (shCtrl+control), 16 (shCtrl+2h Bic/4AP), 16 (sh13A+control), 15 (sh13A+2h Bic/4AP) videos/condition). **(G)** Percentage of motile STAM1 puncta in axons, showing that the increased motility of STAM1 after 2h Bic/4AP treatment is abolished in sh13A-expressing neurons (***P<0.001, one-way ANOVA with Sidak's multiple comparisons test; ≥3 weeks of replicates, n=14 (shCtrl+control), 15 (shCtrl+2h Bic/4AP), 13 (sh13A+control), 13 (sh13A+2h Bic/4AP) videos/condition). Images and kymographs of mCh-STAM1 puncta under these conditions are shown in Fig. S6D-E. All scatter plots show mean ± SEM.

Video 8. Hrs exhibits increased motility in response to neuronal firing in shCtrl-expressing microfluidically-isolated axons. EGFP-Hrs puncta, soma to the right. One frame every 5 seconds, playback is 5x real time. Still image from video is in Fig. 7D.

Video 9. Hrs does not exhibit increased motility in response to neuronal firing in sh13A-expressing microfluidically-isolated axons. EGFP-Hrs puncta, soma to the right. One frame every 5 seconds, playback is 5x real time. Still image from video is in Fig. 7E.

Figure 8. Model of how activity stimulates the increase in transport of ESCRT-0+ vesicles. We hypothesize that neuronal firing increases the association of axonal ESCRT-0-positive vesicles with plus-end directed kinesin KIF13A. Over time, this leads to an increase in

anterograde transport of these vesicles, which deliver Hrs and STAM1 to SV pools in order to mediate the activity-dependent degradation of SV proteins.

Figure 1

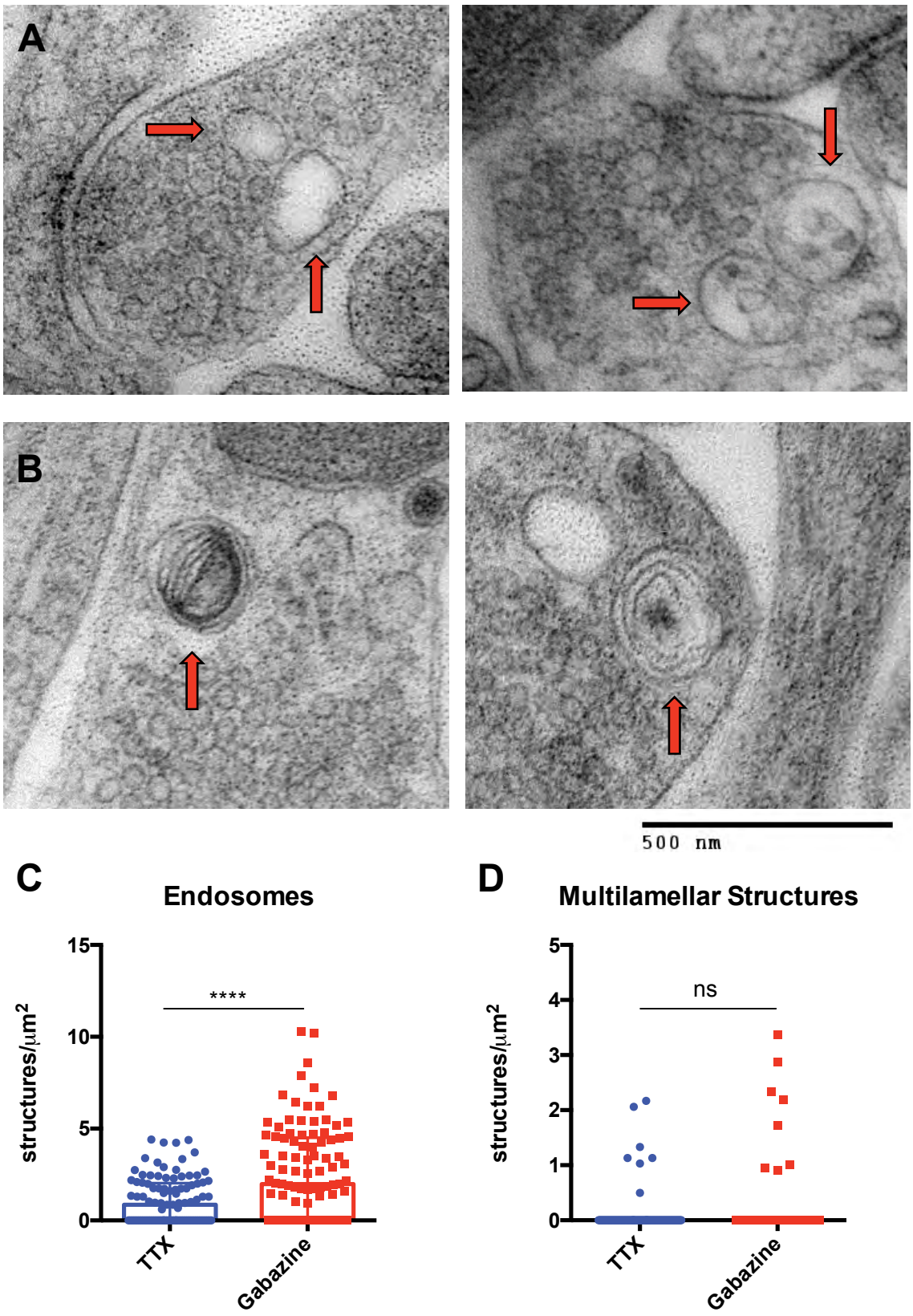
A
B
500 nm
C
Endosomes
structures/μm²
15
10
5
0
****
TTX
Gabazine
D
Multilamellar Structures
structures/μm²
5
4
3
2
1
0
ns
TTX
Gabazine

Figure 2

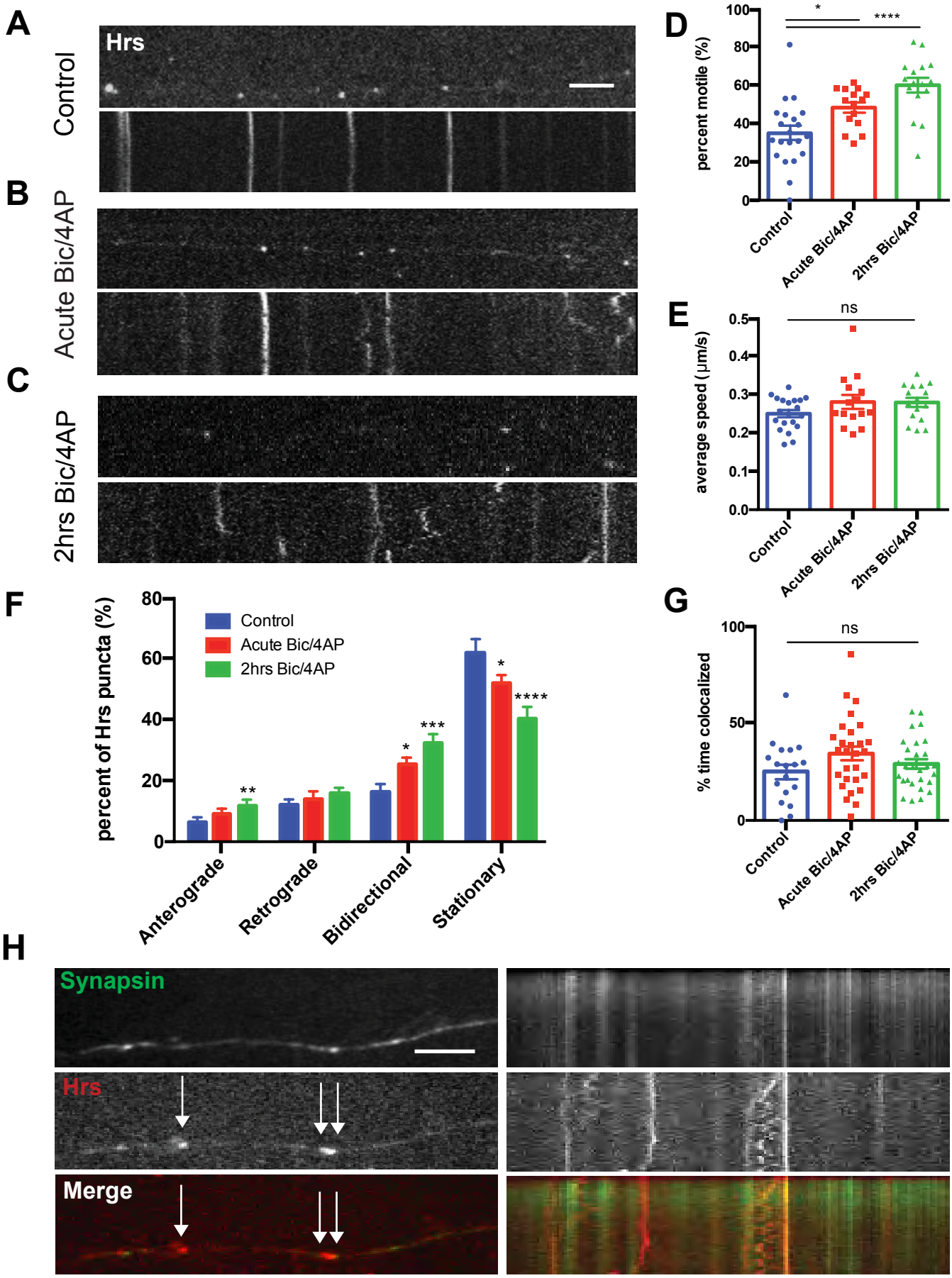
A
Hrs
Control
B
Acute Bic/4AP
C
2hrs Bic/4AP
D
percent motile (%)
100
80
60
40
20
0
*
****
Control
Acute Bic/4AP
2hrs Bic/4AP
E
average speed (µm/s)
0.5
0.4
0.3
0.2
0.1
0.0
ns
Control
Acute Bic/4AP
2hrs Bic/4AP
F
percent of Hrs puncta (%)
80
60
40
20
0
Control
Acute Bic/4AP
2hrs Bic/4AP
**
*
***
*
****
Anterograde
Retrograde
Bidirectional
Stationary
G
% time colocalized
100
50
0
ns
Control
Acute Bic/4AP
2hrs Bic/4AP
H
Synapsin
Hrs
Merge

Figure 3

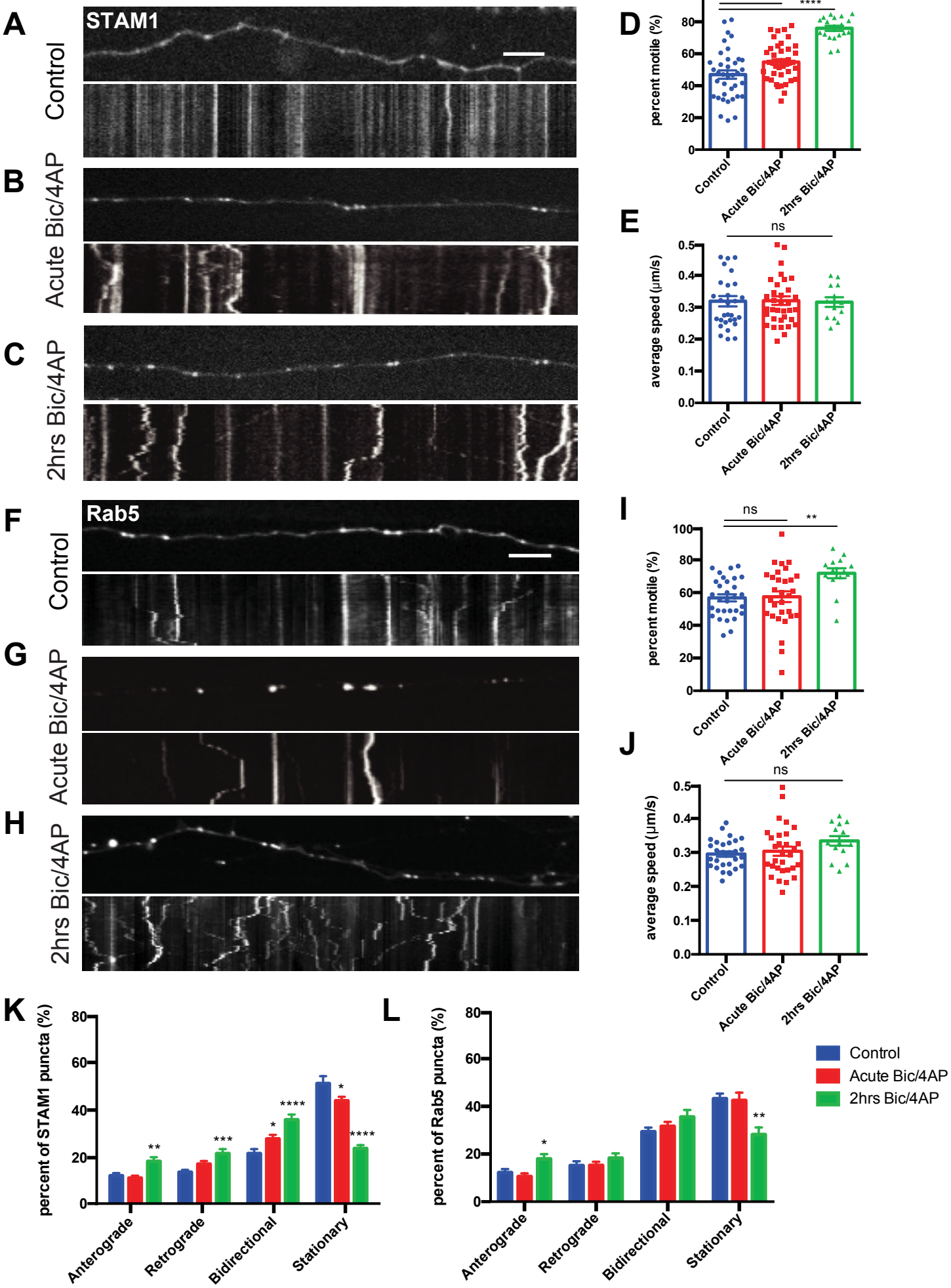
A
STAM1
Control
B
Acute Bic/4AP
C
2hrs Bic/4AP
D
percent motile (%)
Control
Acute Bic/4AP
2hrs Bic/4AP
E
ns
average speed (µm/s)
F
Rab5
G
H
I
J
K
percent of STAM1 puncta (%)
Anterograde
Retrograde
Bidirectional
Stationary
L
percent of Rab5 puncta (%)
Control
Acute Bic/4AP
2hrs Bic/4AP

Figure 4

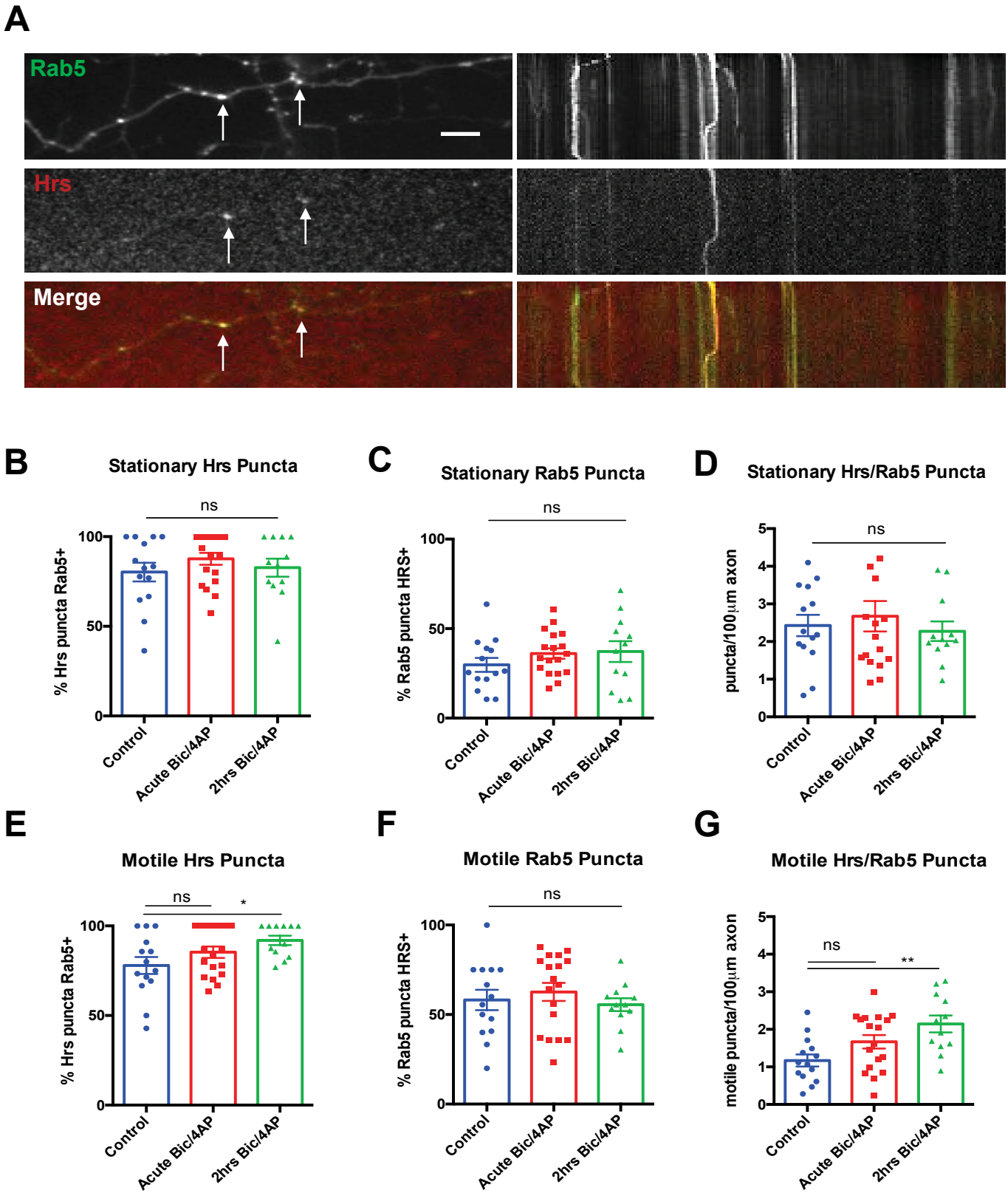
A
Rab5
Hrs
Merge
B
Stationary Hrs Puncta
% Hrs puncta Rab5+
ns
Control
Acute Bic/4AP
2hrs Bic/4AP
C
Stationary Rab5 Puncta
% Rab5 puncta HRS+
ns
D
Stationary Hrs/Rab5 Puncta
puncta/100μm axon
ns
E
Motile Hrs Puncta
% Hrs puncta Rab5+
ns
*
F
Motile Rab5 Puncta
% Rab5 puncta HRS+
ns
G
Motile Hrs/Rab5 Puncta
motile puncta/100μm axon
ns
**

Figure 5

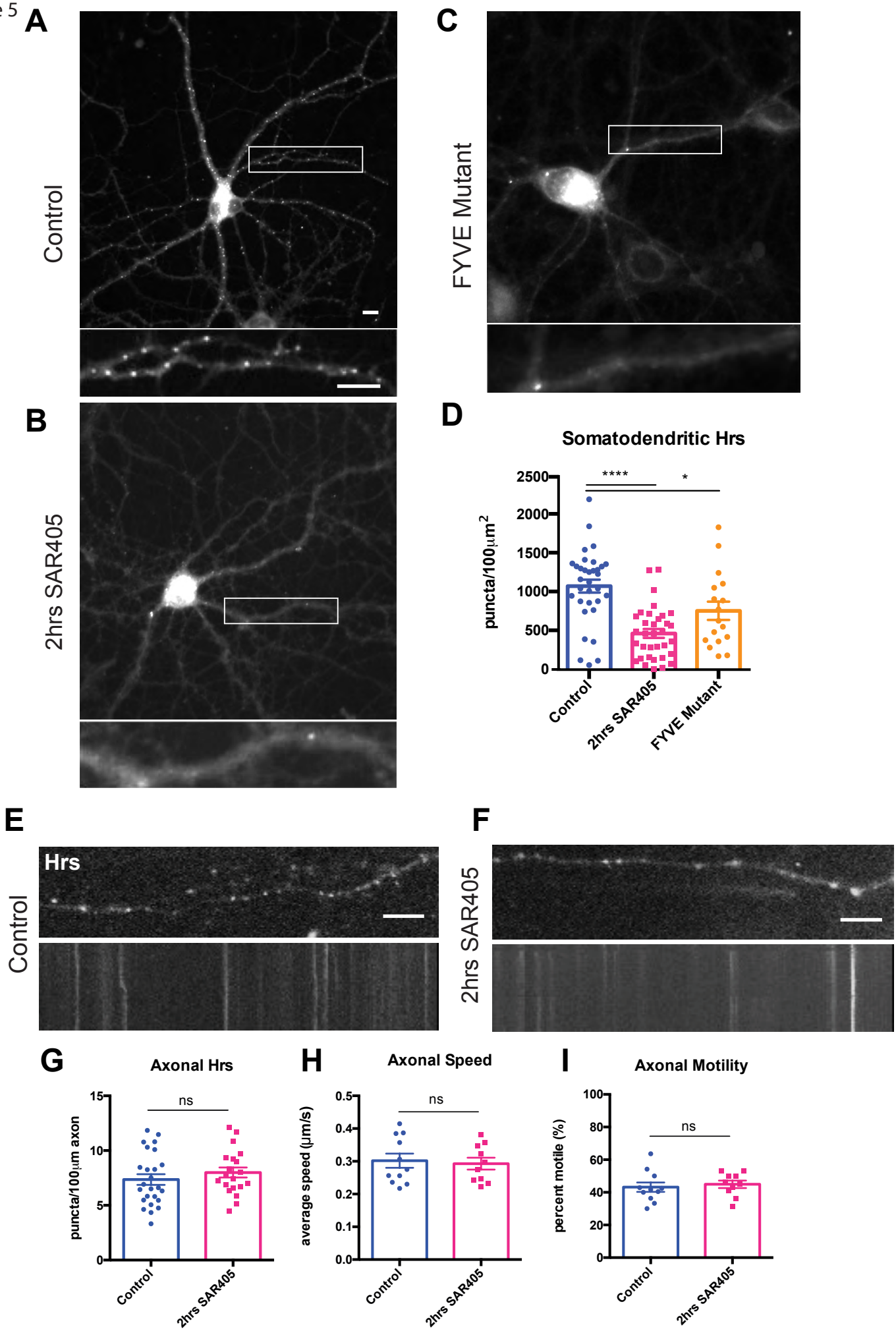
A
Control
C
FYVE Mutant
B
2hrs SAR405
D
Somatodendritic Hrs
puncta/100μm2
2500
2000
1500
1000
500
0
****
*
Control
2hrs SAR405
FYVE Mutant
E
Hrs
Control
F
2hrs SAR405
G
Axonal Hrs
puncta/100μm axon
15
10
5
0
ns
Control
2hrs SAR405
H
Axonal Speed
average speed (μm/s)
0.5
0.4
0.3
0.2
0.1
0.0
ns
Control
2hrs SAR405
I
Axonal Motility
percent motile (%)
100
80
60
40
20
0
ns
Control
2hrs SAR405

Figure 6

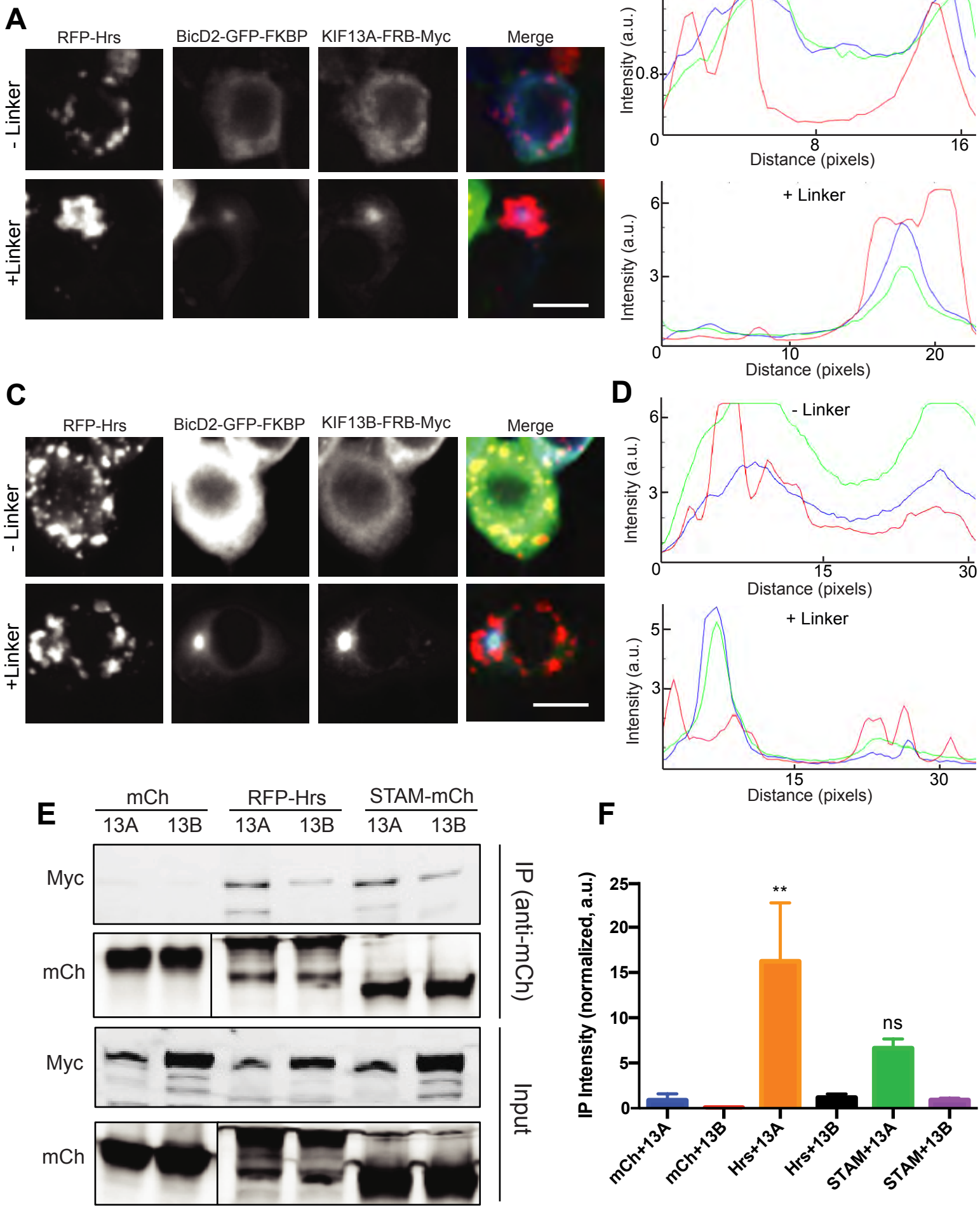
A
RFP-Hrs
BicD2-GFP-FKBP
KIF13A-FRB-Myc
Merge
- Linker
+Linker
B
- Linker
Intensity (a.u.)
Distance (pixels)
+ Linker
C
RFP-Hrs
BicD2-GFP-FKBP
KIF13B-FRB-Myc
Merge
- Linker
+Linker
D
- Linker
Intensity (a.u.)
Distance (pixels)
+ Linker
E
mCh
RFP-Hrs
STAM-mCh
13A
13B
Myc
mCh
IP (anti-mCh)
Input
F
IP Intensity (normalized, a.u.)
**
ns
mCh+13A
mCh+13B
Hrs+13A
Hrs+13B
STAM+13A
STAM+13B

Figure 7

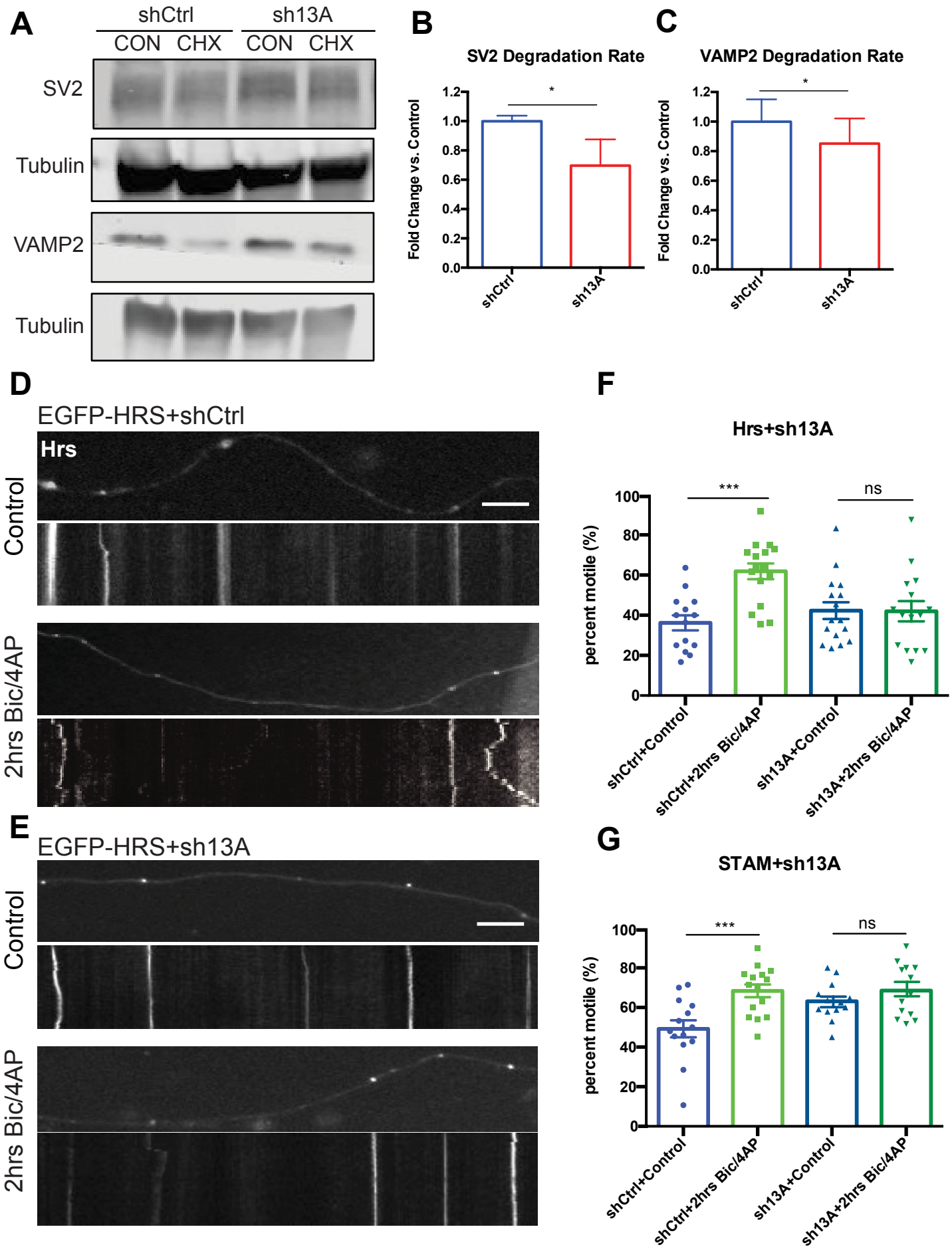
A
shCtrl
sh13A
CON
CHX
CON
CHX
SV2
Tubulin
VAMP2
Tubulin
B
SV2 Degradation Rate
Fold Change vs. Control
1.2
1.0
0.8
0.6
0.4
0.2
0.0
*
shCtrl
sh13A
C
VAMP2 Degradation Rate
Fold Change vs. Control
1.2
1.0
0.8
0.6
0.4
0.2
0.0
*
shCtrl
sh13A
D
EGFP-HRS+shCtrl
Hrs
Control
2hrs Bic/4AP
E
EGFP-HRS+sh13A
Control
2hrs Bic/4AP
F
Hrs+sh13A
percent motile (%)
100
80
60
40
20
0
***
ns
shCtrl+Control
shCtrl+2hrs Bic/4AP
sh13A+Control
sh13A+2hrs Bic/4AP
G
STAM+sh13A
percent motile (%)
100
80
60
40
20
0
***
ns
shCtrl+Control
shCtrl+2hrs Bic/4AP
sh13A+Control
sh13A+2hrs Bic/4AP

Figure 8

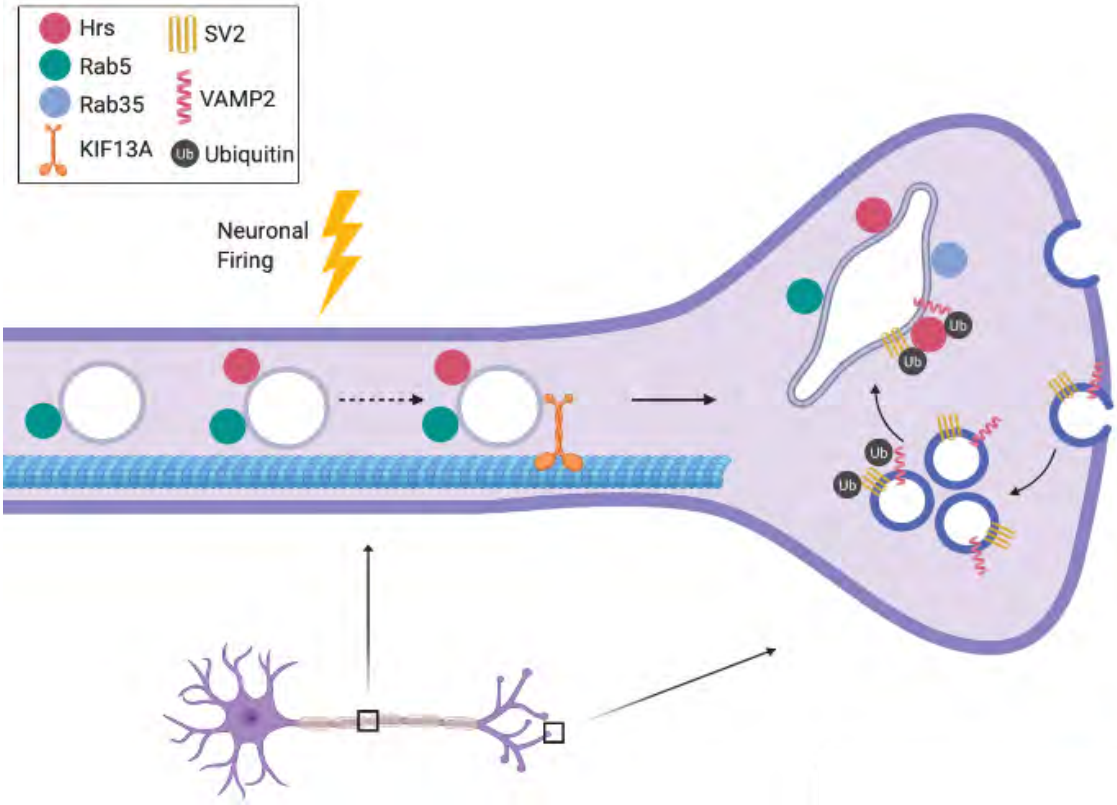
Hrs
Rab5
Rab35
KIF13A
SV2
VAMP2
Ub Ubiquitin
Neuronal
Firing
Ub
Ub
Ub
Ub